

AMERICAN UNIVERSITY OF BEIRUT

PIEZOELECTRIC WAFERS PLACEMENT ON COMPLEX AND
LARGE STRUCTURES BASED ON GENETIC ALGORITHM

by

ZAINAB MOHAMMAD ISMAIL

A thesis
submitted in partial fulfillment of the requirements
for the degree of Master of Engineering
to the Department of Mechanical Engineering
of the Faculty of Engineering and Architecture
at the American University of Beirut

Beirut, Lebanon
April 2019

AMERICAN UNIVERSITY OF BEIRUT

PIEZOELECTRIC WAFERS PLACEMENT ON COMPLEX AND
LARGE STRUCTURES BASED ON GENETIC ALGORITHM

by
ZAINAB MOHAMMAD ISMAIL

Approved by:

Dr. Samir Mustapha, Assistant Professor
Department of Mechanical Engineering
Maroun Semaan Faculty of Engineering and Architecture
American University of Beirut



Advisor

Dr. Hussein Tarhini, Assistant Professor
Department of Industrial Engineering
Maroun Semaan Faculty of Engineering and Architecture
American University of Beirut



Member of Committee

Dr. Mohammad Harb, Assistant Professor
Department of Mechanical Engineering
Maroun Semaan Faculty of Engineering and Architecture
American University of Beirut



Member of Committee

Date of thesis defense: April 25, 2019

AMERICAN UNIVERSITY OF BEIRUT

THESIS, DISSERTATION, PROJECT RELEASE FORM

Student Name: Ismail Zainab Mohammed
Last First Middle

Master's Thesis Master's Project Doctoral Dissertation

I authorize the American University of Beirut to: (a) reproduce hard or electronic copies of my thesis, dissertation, or project; (b) include such copies in the archives and digital repositories of the University; and (c) make freely available such copies to third parties for research or educational purposes.

I authorize the American University of Beirut, to: (a) reproduce hard or electronic copies of it; (b) include such copies in the archives and digital repositories of the University; and (c) make freely available such copies to third parties for research or educational purposes after:

One — year from the date of submission of my thesis, dissertation, or project.

Two — years from the date of submission of my thesis, dissertation, or project.

Three — years from the date of submission of my thesis, dissertation, or project.

 May 2, 2019

Signature

Date

ACKNOWLEDGMENT

To the light, my God, who guided me through the way and led me to accomplish this fine work, goes my greatest and faithful thanks.

Special thanks are for my thesis advisor Dr. Samir Mustapha who provided me with all his support and care. The door to Prof. Mustapha was always open whenever I ran into a trouble spot or had a question about my research and writing.

I would like also to thank Dr. Hussein Tarhini for his academic support and advice. He was always happy to help, guide, and encourage me.

Many thanks and appreciation are for all those who provided any technical and research support as:

- Mr. Mohammad Ali Fakih who had his own contribution in the research work done.
- Mr. Mohammad Mahdi Alloush for his help in providing some Matlab codes.
- MEA for providing the Airbus A330 cargo door.

The most special thanks and love are for those who are always there for me, those who have borne and will always bear all the difficulties to stand by my side, those whom no matter how much I thank, I will never pay them back, for my supporting friends, for my tender family, for my precious parents, for my adorable husband, and for my lovely son.

To every person who gave me something to light my pathway, I thank him for believing in me.

AN ABSTRACT OF THE THESIS OF

Zainab Mohammad Ismail for

Master of Engineering

Major: Mechanical Engineering

Title: Piezoelectric Wafers Placement on Complex and Large Structures Based on Genetic Algorithm

This study presents an effective solution for the optimization of piezoelectric (PZT) wafers placement in a network on convex and non-convex structures, towards the application in the field of structural health monitoring. The proposed objective function is to maximize the coverage of the monitored area, discretized by a set of control points while minimizing the number of PZT wafers. In the optimum solution, each control point should be covered by a user-defined number of sensing paths, defined as the coverage level. The PZT locations were treated as continuous variables. Thus, during the optimization process, any location on the plate is considered as a potential position for a PZT wafer.

The algorithm provides the flexibility of changing a wide range of parameters including the number of PZT wafers, the distance covered around the sensing path, the required coverage level and the number of control points, in addition to identifying the most sensitive PZT wafer within the network. The tractability of the model proposed was improved by feeding the solver an initial solution. The model calculates the importance of each PZT wafer within the network, which allows for further reduction of the number of active PZT elements. The suggested model was solved using a genetic algorithm.

Multiple sensor network configurations on composite and metallic structures were selected, including a large cargo door of an A330 airplane, and validated experimentally. The experimental validation was to evaluate the accuracy in damage localization within the optimized sensor networks. The results demonstrated the proficiency of the model developed in distributing the PZT wafers on non-convex structures and large metallic structures.

CONTENTS

ACKNOWLEDGMENT	v
ABSTRACT	vi
ILLUSTRATIONS	ix
TABLE	xi
Chapter	
I. INTRODUCTION	1
II. METHODOLOGY	9
A. Introduction.....	9
B. Optimization: Genetic Algorithm	12
C. Problem formulation.....	14
1.Parameter notation	14
2.Decision variables.....	15
3.Models	15
III. SIMULATED CASES: RESULTS AND DISCUSSION	
.....	18
A. Composite sandwich structure.....	18
B. Airbus A330 cargo door	27
1.Sub-structure optimization.....	28
2.Optimization over the whole structure	35
IV. EXPERIMENTAL VALIDATION.....	37
A. Experiment set-up	37
1.Composite sandwich structure.....	37
2.Airbus A330 cargo door	40

B.	Experimental results	42
1.	Data fusion	42
2.	Damage localization- composite sandwich structure	45
3.	Damage localization- Airbus A330 cargo door	50
V.	GRAPHICAL USER INTERFACE	54
A.	Geometry	54
B.	Wave properties	55
C.	Preliminary configuration	56
D.	Aimed coverage	56
E.	Optimization	57
F.	Export results	57
G.	Results and plots	58
VI.	CONCLUSIONS	61
	REFERENCES	63

ILLUSTRATIONS

Figure	Page
1. A sketch illustrating the optimization model constraints and terminology	10
2. A flowchart showing the model process	11
3. A flowchart showing the GA process	13
4. An illustration explaining the triangular inequality equations.....	17
5. Square panel sensor network: (a) preliminary configuration, and (b) optimized solution.....	20
6. T-shaped panel sensor network: (a) preliminary configuration, and (b) optimized solution.....	21
7. The variation of the coverage versus the number of sensors tried during the optimization process: (a) square panel and (b) T-shaped panel.....	22
8. Histograms of the mean coverage percentage with error bars (of the 10 trials) for different numbers of sensors: (a) square panel and (b) T-shaped panel	23
9. (a) Coverage after removing each sensor, (b) the normalized importance of the sensors.....	24
10. After removing sensor 12 (a) Coverage after removing each sensor, (b) the normalized importance of the sensors	25
11. The selected sensor network on the square plate	26
12. Standard deviation of the coverage when moving each sensor	27
13. Airbus A330-200 cargo door position and dimensions [41].....	28
14. Cargo door partitions	29
15. Preliminary sensor networks of: (a) partition A, (b) partition B, (c) partition C, (d) partition D, and (e) partition E.....	31
16. Optimized sensor networks of: (a) partition A, (b) partition B, (c) partition C, (d) partition D, and (e) partition E.....	32
17. Combined sensor networks after reducing the PZTs from 165 to: (a) 100 sensors then (b) 70 sensors	33

18. First approach's optimized sensor network, achieving 94% coverage, with a propagation distance and number of sensors of (a) 1 meter- 70 sensors and (b) 1.5 meters- 46 sensors.....	35
19. Second approach's 70-sensor networks: (a) preliminary and (b) optimized solutions.....	36
20. A photo of the tested composite sandwich plate.....	38
21. A schematic diagram of the experimental setup.....	38
22. (a) Cargo door and (b) Section D sensor network	41
23. Damage localization of damage 1 on the square panel with the two circular holes at (a) 200 kHz and (b) 250 kHz	46
24. Damage localization of damage 2 on the square panel with the two circular holes at (a) 200 kHz and (b) 250 kHz	47
25. Damage localization of damage 3 on the square panel with the two circular holes at (a) 200 kHz and (b) 250 kHz	48
26. After removing some sensors: (a) the covered and covered regions, and (b) damage 3 prediction at 200 kHz	49
27. Damage localization, using an excitation frequency of 300 kHz on section D of damage 1	51
28. Damage localization, using an excitation frequency of 300 kHz on section D of damage 2	51
29. Damage localization, using an excitation frequency of 300 kHz on section D of damage 3	52
30. GUI- Geometry panel	55
31. GUI- Wave properties panel	55
32. GUI- Preliminary configuration panel.....	56
33. GUI- Aimed coverage panel	57
34. GUI- Optimization panel	57
35. GUI- Export results panel	58
36. GUI- Results and plots panel	59
37. A screenshot of the GUI	60

TABLES

Table	Page
1. Optimized locations of the PZT wafers on the square panel	40
2. Optimized locations of the PZT wafers on the cargo door	42
3. Damage scenarios and predicted locations using an excitation frequency of 200 and 250.....	50
4. Damage scenarios and predicted locations using an excitation frequency of 300 kHz.....	53

CHAPTER I

INTRODUCTION

The development of continuous structural monitoring systems in aerospace, mechanical and civil structures would form a major establishment in the field of damage detection, assessment, and failure prediction. Knowing the integrity of in-service structures, on a continuous real-time basis, is crucial for manufacturers, end-users and maintenance teams. Structural health monitoring (SHM) is an area of growing interest and worthy of new and innovative approaches. Continuous monitoring requires the constant collection of data from sensors that are embedded within the structure. The data can then be analyzed to detect the presence of any possible flaws. The number of sensors needed to cover a structure and their placement is associated with many challenges, i.e., they depend on the type of data collected (vibration, strain, etc.) and the approach adopted for data analysis.

The technological developments of piezoelectric (PZT) transducers, gives the possibility to develop effective and robust SHM systems for damage detection in composite and metallic components without affecting the performance of the structure [1, 2]. An important feature of PZT transducers is their electro-mechanical coupling which makes them particularly suitable as sensors and actuators in both passive [3] and active sensing [4, 5]. Lamb-waves have been extensively studied for damage detection in recent years due to their sensitivity to different types of damage and their ability to propagate for long distances [6, 7].

PZT wafer placement in a network, in an optimal configuration, is vital to ensure full coverage of the area under-study while minimizing the number of elements used within the network. Various metaheuristic optimization algorithms exist in the literature, for sensor placement, with many common foundations [8, 9]. They implement a form of stochastic optimization so that the solution found is dependent on the set of random variables generated [10]. In combinatorial optimization, by searching over a large set of feasible solutions, metaheuristics can often find good solutions with less computational effort than iterative methods or simple heuristics [10]. As such, they are useful approaches for optimization problems. Padula and Kincaid [9] have discussed some sample applications from NASA Langley Research Center, and tested different optimization methods on them. The algorithms for optimal placement of actuators and sensors appear to be very similar regardless of the application. All can be posed as selecting a subset of locations from a large set of candidate locations. Padula et al. described several combinatorial optimization methods like Tabu Search, Simulated Annealing, and Genetic algorithms that are effective in solving these problems.

Previous research findings on the performance comparison between Tabu Search TS and Simulated Annealing SA suggest that TS performs better than SA. Battiti and Tecchiolli [11] reported that TS performed better than SA in terms of CPU time needed to reach a solution quality which is 1% from the best known solutions. Another direct comparison between SA and TS was done by Chiang and Chiang [12] where they have compared the performance of SA, TS, Probabilistic TS, and Hybrid TS for solving the facility layout problem, formulated as a Quadratic Assignment Problem QAP. Their results show that their basic TS approach performs better than SA. Sinclair [13] and

Arostegui [14] gave a similar result. In contrast to these results, in an early study Paulli [15] has reported that SA outperforms TS when the same computation time is spent by both algorithms.

Hussin et al. [16] have compared two versions of SA and two versions of TS algorithms. Their experimental design was targeted towards examining the relative performance of these algorithms in dependence of instance size. The strongest dependencies have been observed for instances that were generated to resemble the structure of real-life instances. On the contrary, for other instance classes, such as unstructured instances, TS algorithms were dominating the SA algorithms independent of instance size.

An effective method based on genetic algorithm (GA) has been presented by Jin et al. [17] to minimize the total distance between the sensors, of a wireless sensor network, and the sink (data collector), that allows for an energy efficient and a longer living sensor network. Optimization was achieved by dividing the sensor network into clusters, each having a cluster-head responsible for collecting the data from all the nodes within the cluster. Later on, cluster-heads will transmit the compressed data to the sink. The authors have used the GA-based approach to determine both the number and locations of the cluster-heads, to minimize the communication distance within the sensor network. They have used binary representation in which an individual consists of a number of bits; each bit corresponds to one sensor or node. A “1” means that the corresponding sensor is a cluster-head; otherwise, it is a regular node. Crossover and mutation in individuals give birth to other individuals in the next generation. The candidate individuals in the next generation are selected depending on their fitness that

is a factor increasing with the decrease of distances and number of cluster-heads. When fitness values are close to each other, there is a risk of stagnation; thus the fitness value of each individual is scaled by subtracting the minimum fitness value in each generation. Then, Jin et al. have proposed an improved GA, in which a two-gene-bit crossover and a two-gene-bit mutation are applied on the parent strings. Heinzelman [18], Tillett [19], and Ostrovsky [20] have also worked earlier on minimizing the communication distance for a predetermined number of cluster-heads. Bhondekar et al. [21] have also worked on optimization using GA by clustering the network. They've classified the sensors to three categories X, Y, and Z with high, moderate and low transmission range (and energy consumption) respectively. The algorithm maximizes the coverage field, and number of sensors in a cluster; and on the other hand minimizes the number of sensors out of range, overlaps between clusters, and the network energy giving for each parameter the suitable weight in the fitness function according to the application. For an $L \times L$ sensor plate, the length of the bit string is $2L^2$ as two bits are required to encode four types of sensing nodes i.e. X, Y, Z and inactive nodes. In this bit string the sequence of two bits decides the type of node: 00 being inactive, 01 being X mode, 10 being Y mode and 11 represents Z mode. As the algorithm progresses, it converges to the string giving the minimum fitness. The algorithm was tried on MATLAB, and the best results were recorded. It was noticed the evolution of the field coverage over generations, and the deterioration of the network energy.

Another use of the genetic algorithm was by Chih-Chung Lai et al [22], who have suggested -for the purpose of prolonging the life span of the sensor network- the division of the deployed sensors into maximum number of disjoint subsets of sensors, or

sensor covers, such that each sensor cover can cover all targets and work by turns. This problem can be solved by transformation to a combinatorial optimization problem, disjoint set covers (DSC) that uses integer representation to encode the grouping combination of sensors where each integer corresponds to the number of the sensor cover that the sensor belongs to.

Ting-Hua Yi et al. [23] have used the generalized genetic algorithm in which dual-structure coding method instead of binary coding method is proposed to code the solution. Each chromosome consists of two rows, the upper one holding indices from 1 to n , and the lower having 0 and 1 only; 1 at the j^{th} position means there is a sensor at this position and 0 means that there are no sensors. Only the upper row is changed, and the lower row is kept fixed so that we can keep the number of sensors constant. In generalized genetic algorithm GGA, another advantage over simple genetic algorithm SGA is that the two parents can also compete with their offspring to avoid premature convergence. Guo et al. [24] presented an improved GA for optimal sensors placement of a metallic truss structure in which two-gene-bit crossover and two-gene-bit mutation are applied on the parent strings. Each string consists of n bits in which q of them should be 1 (1 means a sensor exists in this position, we need to allocate q sensors).

Mallardo et al. [25] have presented a passive sensing algorithm based on GA and Artificial Neural Network (ANN) techniques, to optimize sensor-positions for impact detection on composite structures. The optimization process took into consideration the uncertainty due to environmental conditions and the possibility of malfunctioning of one or more sensors. Flynn and Todd [26] proposed an approach for an optimal actuator and sensor placement for active sensing-based SHM. Using a

detection theory framework, they established the optimum configuration as the one that minimizes Bayes risk. The detector incorporates a statistical model of the active sensing process that accounts for both reflection and attenuation features and implements pulse-echo and pitch-catch actuation schemes and takes into account the line-of-sight. The optimization space was searched using GA with a time-varying mutation rate. For verification, they instrumented a concave-shaped plate and applied artificial, reversible damage to a large number of randomly generated locations, acquiring active sensing data for each location. Then, they used the algorithm to predict the optimal subsets of the dense array. The predicted optimal arrangements proved to be among the top performers when compared to large sets of randomly generated arrangements.

Schoefs et al. [27] proposed a methodology to optimize the spatial distribution of embedded sensors used for spatial variability assessment of stationary random fields. The optimization criterion relies on the width of the confidence interval of statistics for the characteristics to identify.

Worden and Burrows [28] compared different optimization approaches for fault detection in a rectangular plate. The objective function used in the optimization was selected for a fault detection procedure based on ANN. A similar approach based on GA was proposed for passive sensing [29]. The proposed optimization algorithms for passive sensing maximize a fitness function which is based on the probability of detection (POD) of the proposed impact detection method [30]. In a study by Croxford et al. [31], the effect of the pattern of sensor layout (i.e., triangle, rectangle, trapezoid) was investigated, and it was found that a square or hexagon configuration provided a close to optimum performance. Yi et al. [32] proposed a novel optimal triaxial sensor

placement approach and a novel distributed wolf algorithm to improve the optimization performance in identifying the best sensor locations. Thiene et al. [33] proposed a sensor placement optimization approach for guided wave fault detection and localization techniques based on maximum area coverage (MAC) within a sensor network. The advantage of this approach is that it is independent of the details of the damage detection algorithm and does not require any determination of a POD function for a vast number of damage scenarios. Moreover, it can be applied to geometrically complex structures with pitch-catch sensor configuration and any active sensing procedure based on time of flight (ToF) of damage reflected waves. Experimental verifications on a flat composite panel, in which BVID was introduced, were conducted. A full probabilistic method based on the Bayesian inverse problem was proposed by Cantero-Chinchilla et al. [34] to rigorously provide a robust estimate of the time of flight for each sensor independently. Then, the prediction was introduced as an input to the Bayesian inverse problem of damage localization. Manohar et al. [35] explored optimized sensor placement for signal reconstruction based on a tailored library of features extracted from training data. Moreover, Zhang et al. [36] explored the fundamental limits of a sensor network lifetime.

In this study, we aimed at designing a framework for sensor network optimization to capture the mathematical model based on the pitch-catch configuration. Several aspects were explored including the modeling of the geometry (represented by a set of control points) and the definition of the PZT locations that were treated as continuous variables. A novel model for PZT-wafer-placement optimization was developed. The objective function of the algorithm was to maximize the coverage of the

monitored area to a predefined level of coverage. During the optimization process, any location on the plate is considered as a potential position for a PZT wafer. The model takes into account several practical constraints such as the attenuation and the coverage of the excited wave. Since GA was proven to be effective in sensor optimization problems, it was adopted in this study and further validated on non-convex surfaces with different shapes and a large metallic structure. A sensitivity study was done to determine how much important each PZT wafer is, and thus indicate sensitive PZTs that should be frequently checked or supported by additional neighboring PZTs.

CHAPTER II

METHODOLOGY

A. Introduction

The proposed optimization algorithm aims to maximize the coverage of a predefined finite set of control points. The coverage level (n), which is a parameter chosen according to the user's requirements, is defined as the number of sensing paths required to cover a control point in order to be considered as covered. Huang and Tseng [37] stated that an accurate damage localization requires the coverage of three sensing paths ($n = 3$), according to triangulation protocols. A sensing path (defined by any pair of PZTs) covers a control point if it lies within a given distance from the centerline of the path. This distance is referred to as the path coverage (z) and was set to 30 or 40 mm (depending on the material) based on literature [38-40]. Other constraints included the plate's geometry, the number of available PZT wafers (N), the minimum distance between each two PZTs ($d_{min} = z$) to avoid having multiple PZTs at the same location, and the minimum angle between two sensing paths ($\alpha_{min} = 10^\circ$) to ensure that the sensing paths are not collinear. Further, a maximum spacing between the actuator-sensor pair was defined to account for the attenuation in the wave signal, it was set to be less than $d_{effective} = 600$ mm in this case. The geometry of the plate was defined as a polygon having a certain number of vertices. The sensor locations were assumed to be continuous variables, as opposed to Thiene et al. [33] in which finite possible locations,

for the PZT wafers, were predefined. For clarity, a sketch illustrating the model constraints and terminology is presented in Figure 1.

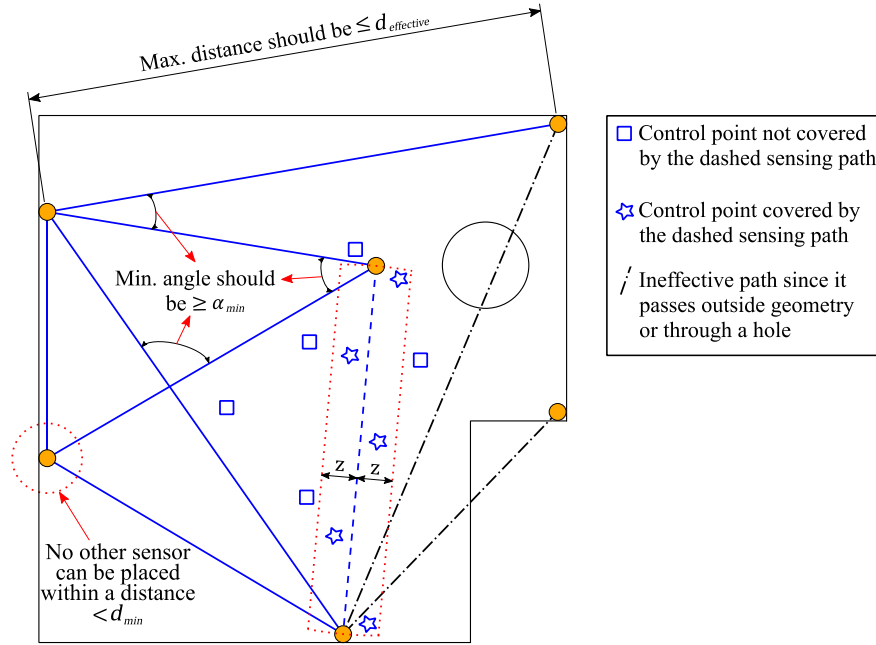


Figure 1. A sketch illustrating the optimization model constraints and terminology

The fitness function, to be maximized, was defined as the percentage of covered control points. Since the problem is a non-convex problem with binary variables, it is impossible to check whether the solution is a local or a global optimum. Thus, to reduce the probability of being stuck on a bad local maximum, a code that generates a preliminary solution and feeds it into the optimization algorithm was developed. The preliminary solution is either a uniform distribution of the available number of sensors along the edges of the plate geometry or evenly distributed through the plate geometry. The algorithm runs automatically for multiple times, through which it changes the number of sensors and calculates the corresponding coverage (Figure 2)

until it reaches the predefined desired coverage (in this study it was set to 95% of the control points) with the least possible number of sensors.

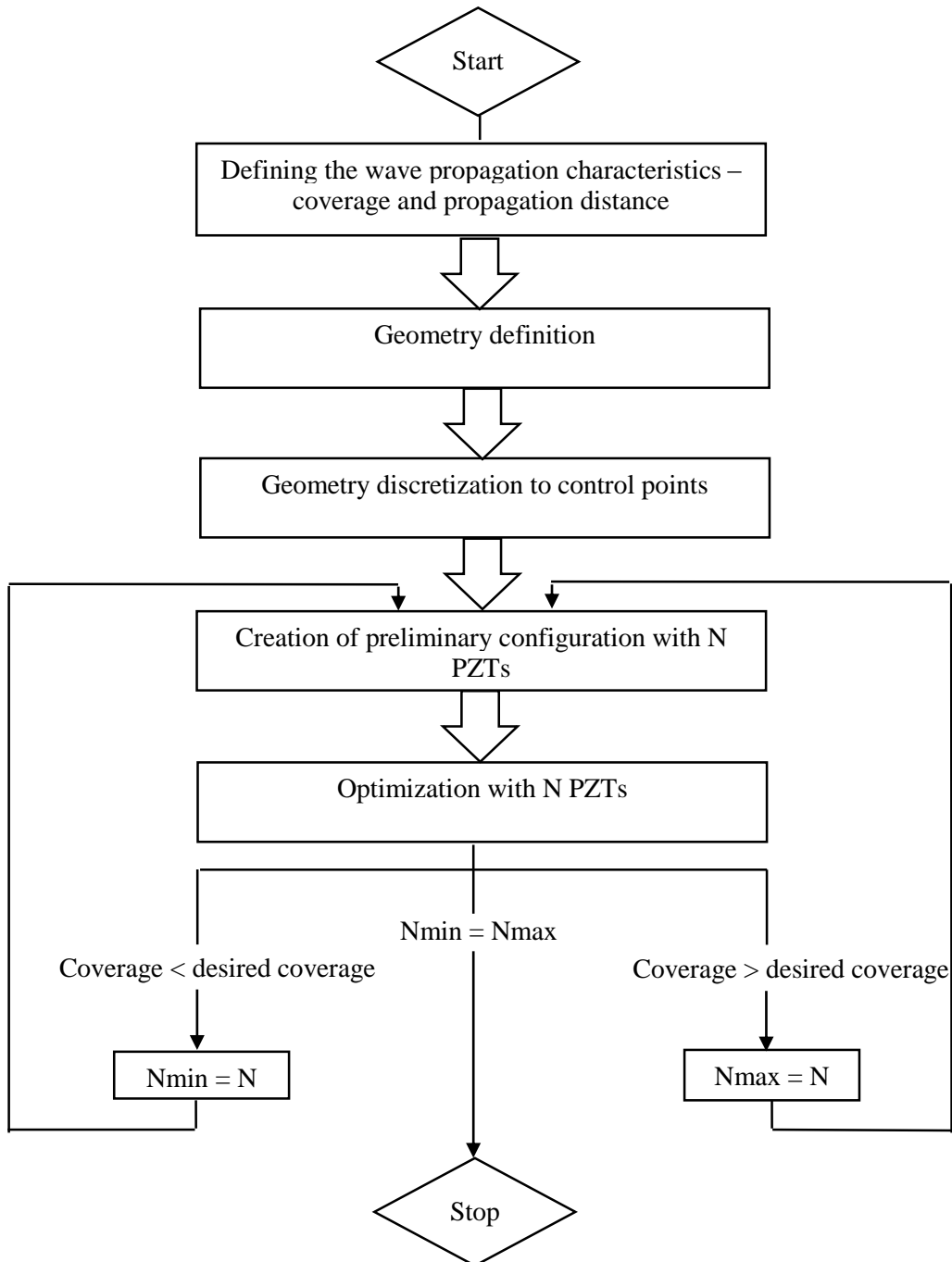


Figure 2. A flowchart showing the model process

B. Optimization: Genetic Algorithm

Genetic Algorithm GA, a metaheuristic inspired by the process of natural selection that belongs to the larger class of evolutionary algorithms, was used to solve the proposed model. A typical GA requires a genetic representation of the solution domain, and a fitness function to evaluate it. Each candidate solution is a chromosome of a number of genes equal to double the number of used PZTs; where each gene is a x or y coordinate value of a PZT element. Besides, the fitness function, to be maximized, is defined as the percentage of covered control points. Once these two elements (the genetic representation and the fitness function) are defined, a GA proceeds to initialize a population of solutions and then improve it through repetitive application of the mutation, crossover, inversion and selection operators (Figure 3). The built-in MATLAB GA function was used with the heuristic crossover function and Gaussian mutation. A population size of 200 was used in each generation to reduce the chance of getting a local optimum. "Rank" scaling function was used to give a scaled fitness value for every single individual in the population. The scaled fitness value of an individual is what defines its probability to be selected as a parent, using the "Stochastic uniform" selection function. The selected parents are used to form a second-generation population of solutions, through a combination of genetic operators including crossover and mutation. Five percent of the population, with the best fitness values, are chosen to pass to the next generation without undergoing crossover and mutation operations (the elite count is 5% of the population size). In the next generation, the average fitness should have increased, since the best organisms from the first generation were mostly selected for breeding, along with a small proportion of less fit solutions.

Less fit solutions could be also produced due to random mutation and crossover between good individuals. However, these solutions ensure genetic diversity within the genetic pool of the parents and therefore ensure the genetic diversity of the subsequent generation of children. The algorithm terminates when a maximum number of generations has been produced, a satisfactory fitness level has been reached for the population, or the highest-ranking solution's fitness has reached a plateau such that successive iterations no longer produce better results.

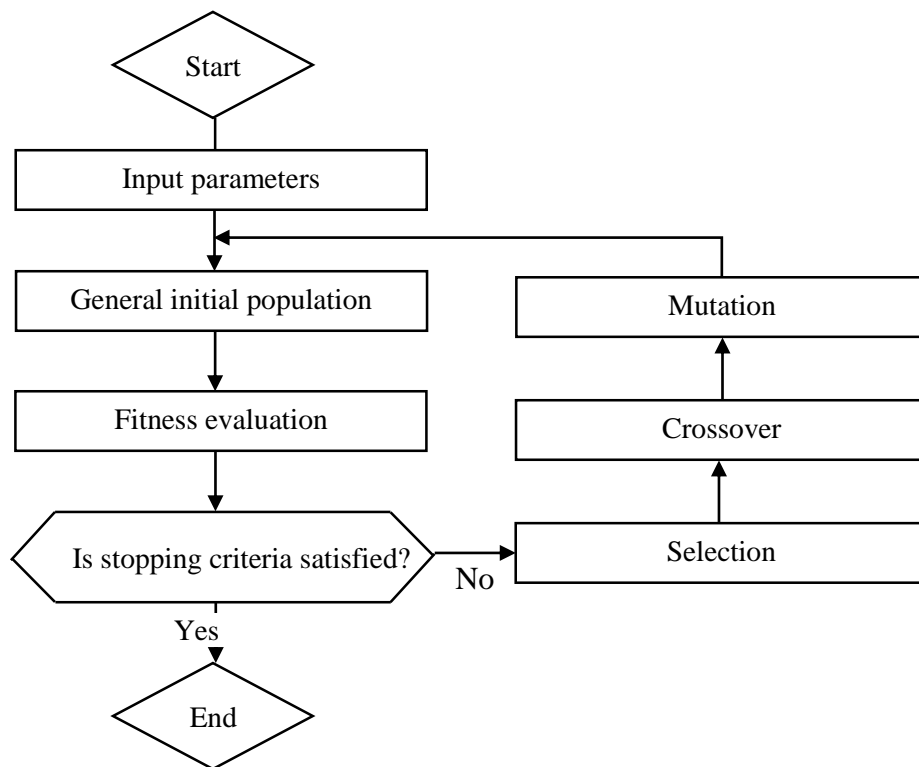


Figure 3. A flowchart showing the GA process

The mutation rate, crossover rate, and population size parameters should be tuned to find reasonable settings for the problem under study. A very small mutation rate may lead to genetic drift (which is non-ergodic in nature), and a very high rate may

lead to the loss of good individuals from the population. When the crossover rate is too high, a premature convergence of the GA may result. A typical crossover rate of 0.8 was taken in this study.

It is worth noting that the optimal solution may change with the selected parameters (including mutation and crossover) and the initial population.

In case the same solution is required to be reproduced, the ‘seed’ which can generate the same pseudo-random number sequence used by GA to create the searching stream, can be used.

C. Problem formulation

The geometry was defined as a polygon having a certain number of vertices.

1. Parameter notation

- K : Set of control points
- (x_k, y_k) : Coordinates of control point k
- N : Number of PZT wafers to be placed
- n : Coverage level
- d_{min} : Minimum distance between each two PZTs
- $d_{effective}$: Maximum spacing between the actuator-sensor pair
- α_{min} : Minimum angle between two sensing paths
- z : Path coverage
- X : Set of points lying inside the geometry of the plate

2. Decision variables

The definitions and equations of the current and the following sections are valid \forall :

$$k \in K; \quad i, j, i_1, j_1, i_2, j_2 \in N; \quad i < j; \quad i_1 < j_1; \quad i_2 < j_2.$$

(x_i, y_i) : Optimized coordinates of PZT wafer i

$$C_k = \begin{cases} 1 & \text{if control point } k \text{ is covered} \\ 0 & \text{otherwise} \end{cases}$$

$$C_{ijk} = \begin{cases} 1 & \text{if control point } k \text{ is covered by PZT wafer line } (i, j) \\ 0 & \text{otherwise} \end{cases}$$

d_{ij} = Distance between PZT wafer i and PZT wafer j

d_{ijk} = Distance between PZT wafer line (i, j) and control point k

d_{ik} = Distance between PZT wafer i and control point k

3. Models

The whole problem is summarized in equations 1 through 12.

$$\max \sum_{k \in K} C_k \tag{1}$$

$$d_{ij}^2 = (x_i - x_j)^2 + (y_i - y_j)^2 \tag{2}$$

$$d_{ik}^2 = (x_i - x_k)^2 + (y_i - y_k)^2 \tag{3}$$

$$d_{ijk} = \frac{|(y_j - y_i) \times x_k - (x_j - x_i) \times y_k + x_j \times y_i - y_j \times x_i|}{\sqrt{(y_j - y_i)^2 + (x_j - x_i)^2}} \tag{4}$$

$$C_{ijk} = 0 \text{ if } d_{ijk} > z \tag{5}$$

$$C_{ijk} = 0 \text{ if } d_{ik} > d_{ij} \tag{6}$$

$$C_{ijk} = 0 \text{ if } d_{jk} > d_{ij} \tag{7}$$

$$C_{ijk} = 0 \text{ if } d_{ij} > d_{effective} \quad (8)$$

$$C_k = 0 \text{ if } \sum_{i \in N} \sum_{j \in N} C_{ijk} < n \quad (9)$$

$$C_{i_1j_1k} + C_{i_2j_2k} \leq 1 \text{ if } \left| \frac{(x_{j_1} - x_{i_1}) \times (x_{j_2} - x_{i_2}) + (y_{j_1} - y_{i_1}) \times (y_{j_2} - y_{i_2})}{\sqrt{((x_{j_1} - x_{i_1})^2 + (y_{j_1} - y_{i_1})^2) \times ((x_{j_2} - x_{i_2})^2 + (y_{j_2} - y_{i_2})^2)}} \right| > \cos \alpha_{min} \quad (10)$$

$$d_{ij} \geq d_{min} \quad (11)$$

$$(x_i, y_i) \in X \quad (12)$$

The objective function is to maximize the number of covered control points as shown in equation (1) where C_k for control point k is 1 if it is covered by the desired coverage level. Equations (2) and (3) calculate the distance between two PZT wafers and the distance between a PZT wafer and a control point k respectively using the simple formula of the distance between two points. Equation (4) calculates the distance between the sensing path (i, j) and the control point k using the simple formula of the distance between a point and a straight line. In equation (5), for a specific control point k to be covered by a path (i, j) , d_{ijk} must be less than the path coverage distance z . Equations (6) and (7) represent the triangular inequality equations between an actuator-sensor pair and a control point. These equations ensure that the control points covered must fall within the range of the sensing path. This is illustrated in

Figure 4 below, where control point k is not covered by path (i, j) although $d_{ijk} < z$ because $d_{jk} > d_{ij}$. Equation (8) disregards all paths longer than $d_{effective}$ because of wave attenuation at long distances. Equation (9) describes the required coverage level for all control points, which is the minimum number of covering sensing paths.

Equation (10) summarizes the minimum angle constraint (α_{min}) which is the angle between each pair of paths to ensure that the sensing paths are not collinear. Equation (11) makes sure that the PZT wafers are separated by a distance $\geq d_{min}$ to avoid having multiple PZTs at the same location. We usually take $d_{min} = z$. Equation (12) defines the plates' geometry, where X is the set of all points lying inside the geometry, and a PZT element can be any point of this set.

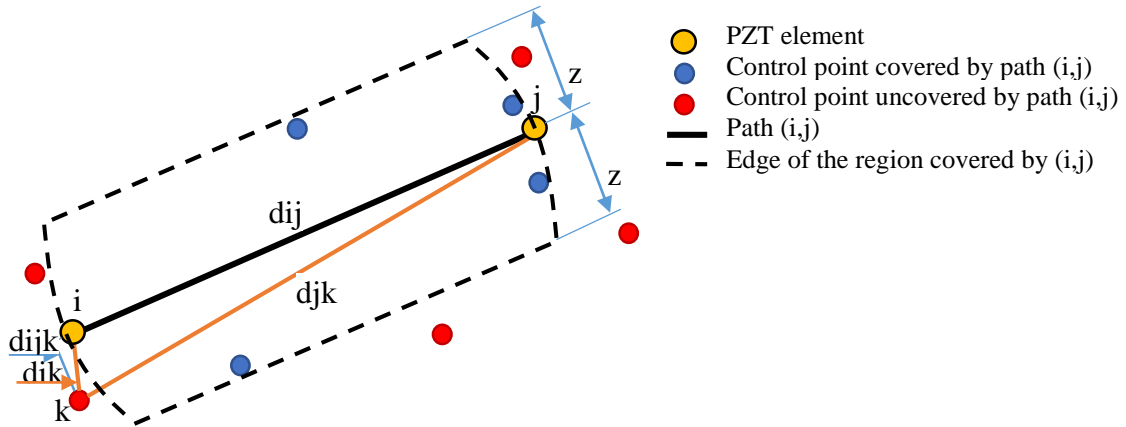


Figure 4. An illustration explaining the triangular inequality equations

CHAPTER III

SIMULATED CASES: RESULTS AND DISCUSSION

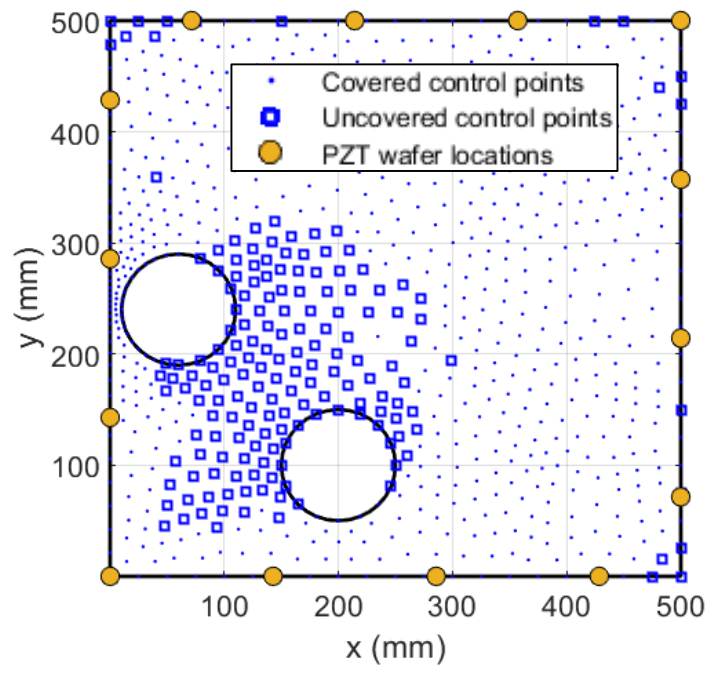
The performance of the model developed was demonstrated on various shapes including a square-shaped panel, a T-section and a large metallic structure (the cargo door of an A330 aircraft). The main objective of the presented cases is to demonstrate the robustness of the method in PZT wafer placement. The parameter n is a user defined attribute that can be controlled to achieve any level of coverage. Level 3 ($n = 3$) optimization was chosen, in this case, for a demonstration on non-convex plates.

A. Composite sandwich structure

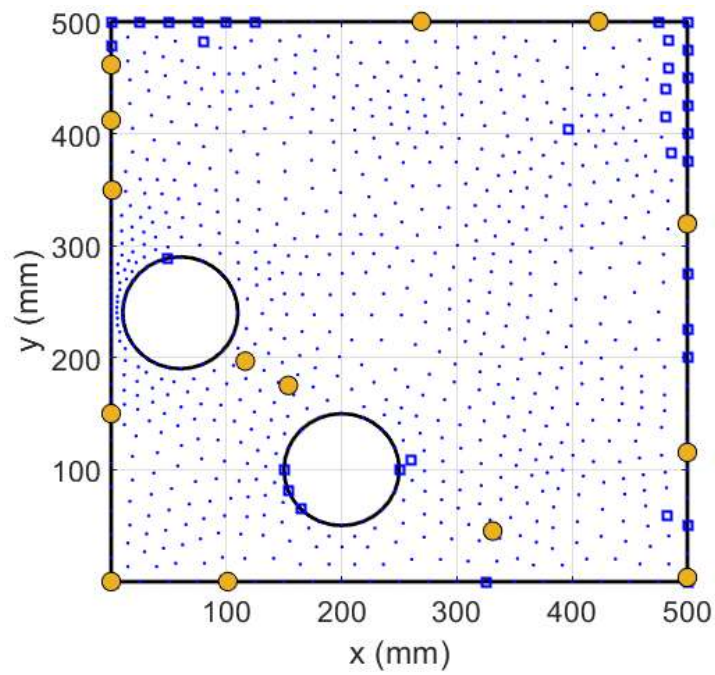
The first plate considered in this study was a composite sandwich structure. For this type of structures, the wave was assumed to propagate for 600 mm and to have a coverage of 40 mm, based on previous experimental studies [38]. Both geometries were selected to be non-convex including a square panel with two circular holes and a T-section. The geometries selected for the sensor networks are shown in Figure 5 (a) and Figure 6 (a) showing the control points randomly distributed to cover the plates, the preliminary solution of the PZT wafers, and the covered control points. During the optimization process, it was assumed that the selected number of sensors is the minimum N giving a coverage of at least 95%.

Starting with the square panel, the optimization algorithm led to a minimum number of $N = 14$ sensors required to achieve a coverage of 96% of 820 control points. However, the coverage of the preliminary solution was below 80% for the same number of sensors. For the T-shaped panel, the preliminary coverage was 84% of 480 control points, while it was found to be 96.5% for the optimized solution, with 12 PZT elements. The covered and uncovered zones for the optimized solutions are shown in Figure 5 (b) and Figure 6 (b). In some cases, several uncovered control points exist in a zone crowded with PZT wafers, due to the fact that the number of sensing paths lying in the neighborhood of a point is not the only indicator of its coverage. However, the angle between each pair of paths and the path length play a main role while calculating the coverage of each point. Referring to Figure 5 (b), three PZT wafers moved towards the region near the holes in the optimized solution, which may be due to the discontinuities. This can also be observed when dealing with large structures, given the limited propagation distance of the wave. Otherwise, placing sensors on the outer boundaries will result in better coverage, which is observed in Figure 6 (b).

Figure 7 (a-b) shows the coverage percentage versus the number of sensors, tried during the optimization process, for the square panel and the T-shaped panel, respectively. The optimized percentage of coverage is increasing with the number of sensors for both plates. It was demonstrated that once a decent coverage is achieved (about 95%), additional sensors may not contribute to a significant improvement in the coverage. Noteworthy coverage improvement was achieved between the initial preliminary solutions and the optimized ones. This indicates the high efficiency of the proposed optimization approach.

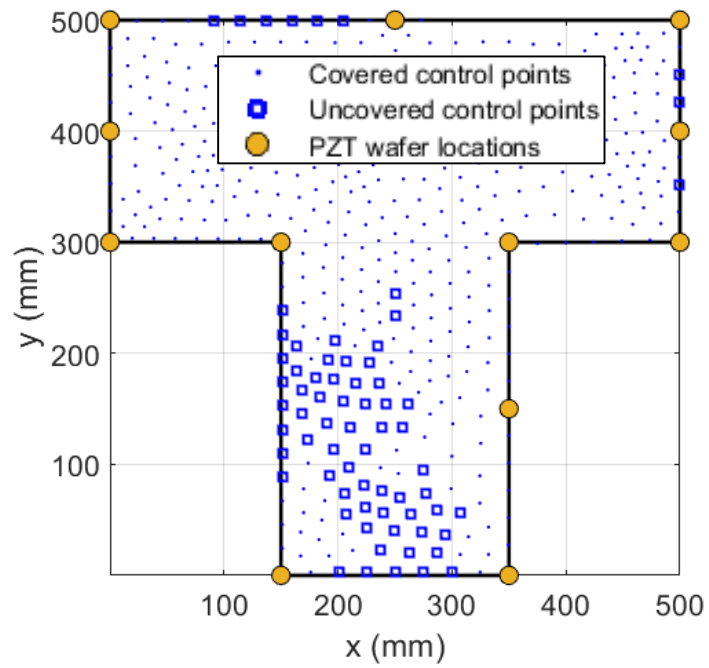


(a)

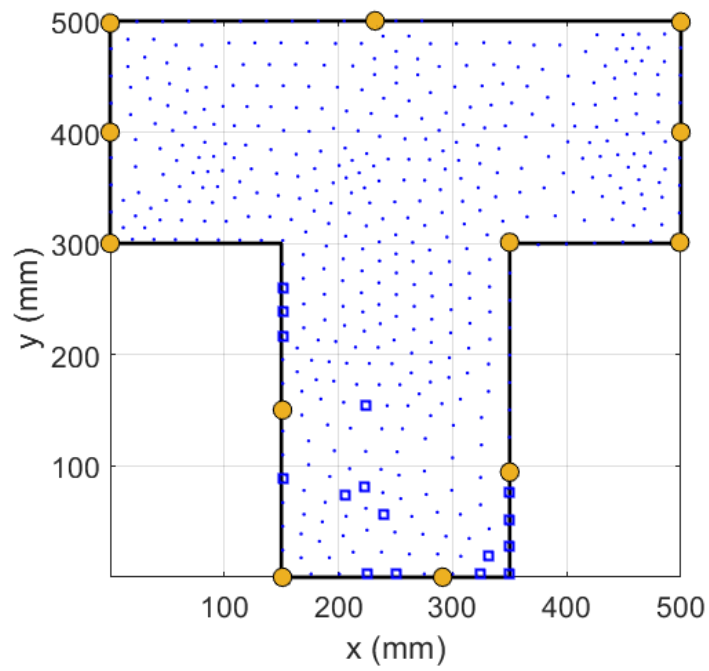


(b)

Figure 5. Square panel sensor network: (a) preliminary configuration, and (b) optimized solution

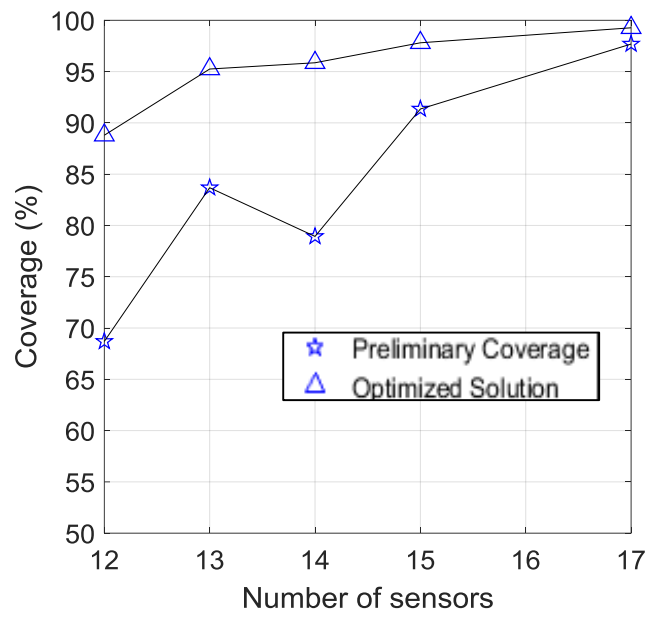


(a)

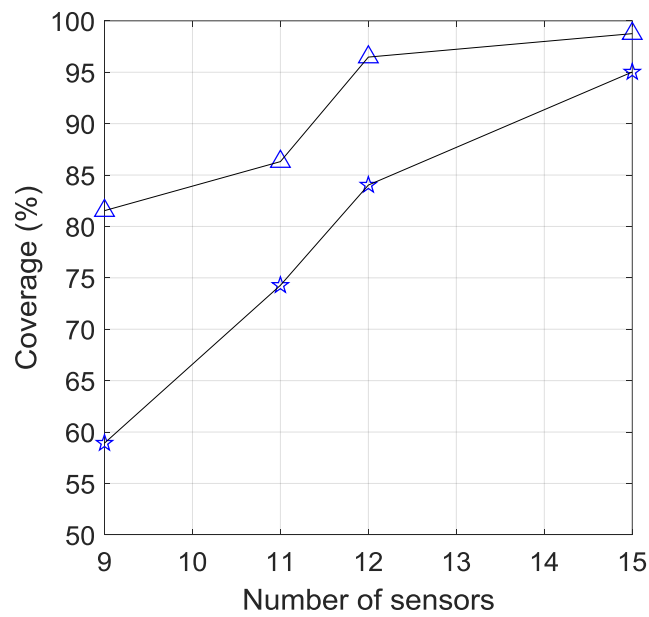


(b)

Figure 6. T-shaped panel sensor network: (a) preliminary configuration, and (b) optimized solution



(a)



(b)

Figure 7. The variation of the coverage versus the number of sensors tried during the optimization process: (a) square panel and (b) T-shaped panel

Furthermore, to check the repeatability of the results, based on the proposed optimization process, a fixed set of N (number of PZT wafers), known to give an optimized coverage percentage above 80%, was chosen for the two different test panels. The optimized sensor network of each value of N (from the chosen set) was computed 10 times, separately. Figure 8 shows the mean coverage percentage, of the two panels, with error bars showing the variation among the 10 trials. A high stability in the percentage coverage was noticed, with a maximum standard deviation of 2.3%. The same procedure is repeated on the square plate; however, the plate was discretized into 100 uniformly distributed control points. The resulting coverage reached 95%, and therefore it was noticed that the number of control points did not significantly affect the coverage. In the meantime, the results of the optimized solution were not repeatable, unlike the cases when a high number of control points is used.

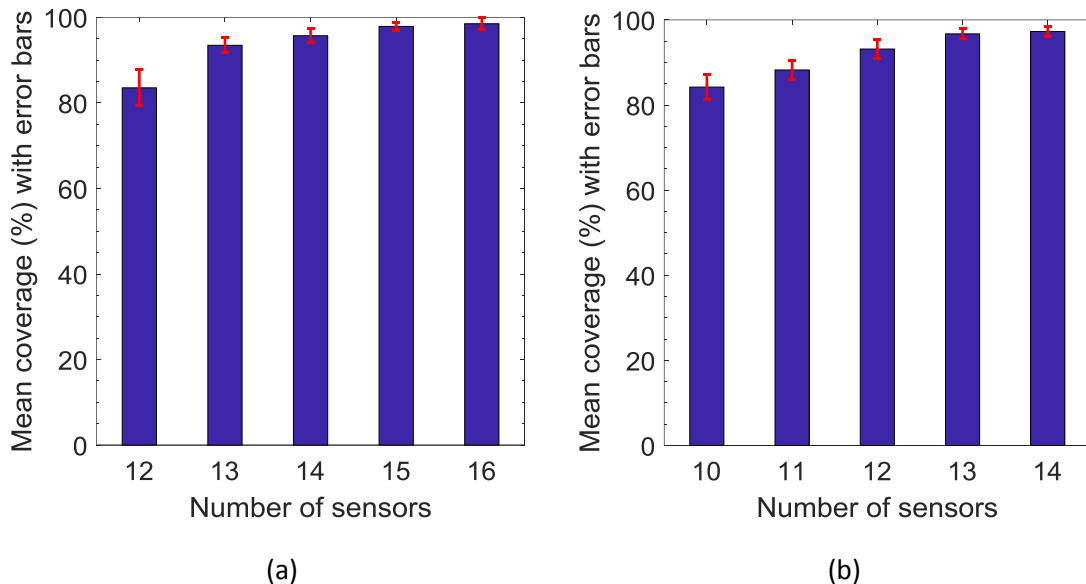


Figure 8. Histograms of the mean coverage percentage with error bars (of the 10 trials) for different numbers of sensors: (a) square panel and (b) T-shaped panel

In addition, sensitivity analysis was performed to determine the importance of each sensor. For each sensor, the drop in coverage level is measured if that sensor is dropped while maintaining the positions of the other sensors, and calculating the corresponding coverage. The process is repeated for all the sensors. The most important sensor is identified as the sensor that caused the maximum drop in coverage.

For the square sensor network (820 control points), the coverage results are presented in Figure 9 (a). The normalized importance of each sensor was calculated, and the results are shown in Figure 9 (b). Sensor 5 was identified as the most important sensor, where the coverage percentage dropped by 15% after its removal.

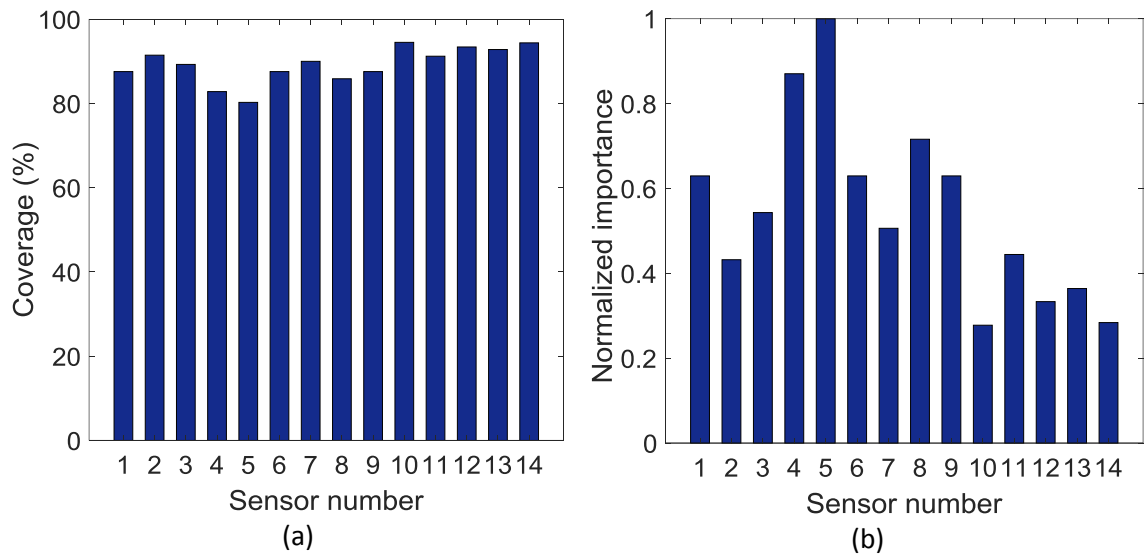


Figure 9. (a) Coverage after removing each sensor, (b) the normalized importance of the sensors

It is worth noting that sensors 12 and 13 although highly improved the coverage when migrated to the area between the holes, however, they appeared to have

relatively low importance values. This is only true when one sensor is removed at a time. In other words, together, sensors 12 and 13, provide a significant improvement in the coverage, and if one of them is removed (for instance sensor 12), the other (sensor 13) will assure adequate coverage, and in this case, it should become an important sensor.

To validate this, sensor 12 was removed from the sensor network, and the sensitivity study was repeated on the rest of the sensors. As expected, sensor 13 became the most important sensor. In addition, the importance of sensors 1, 2, and 14, has increased after the removal of sensor 12 due to their presence in the same region with sensor 12 (as shown in Figure 10 (a-b)).

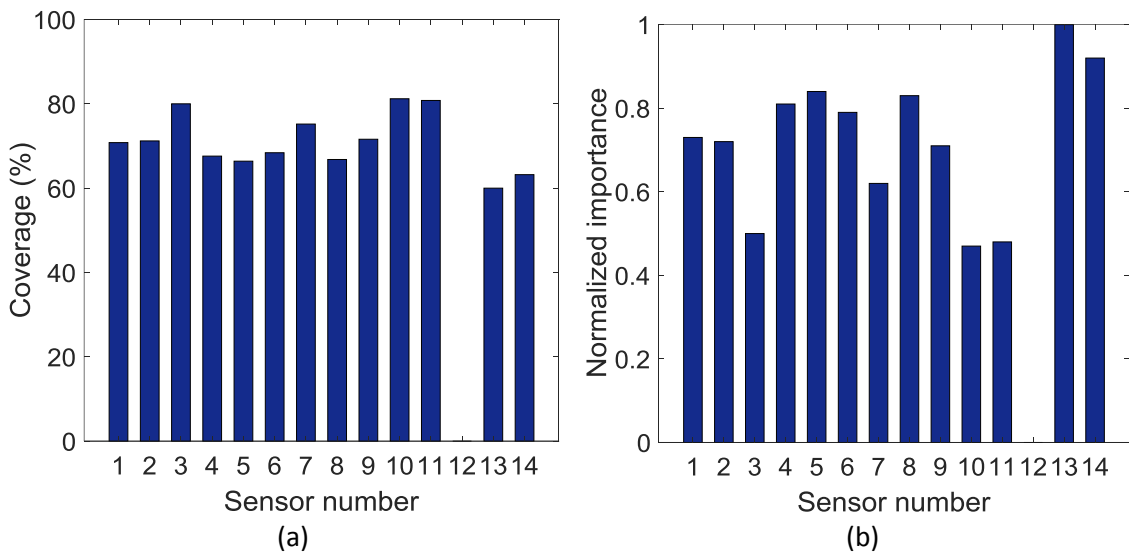


Figure 10. After removing sensor 12 (a) Coverage after removing each sensor, (b) the normalized importance of the sensors

The selected sensor network, on the square plate, that will be experimentally validated is shown in Figure 11.

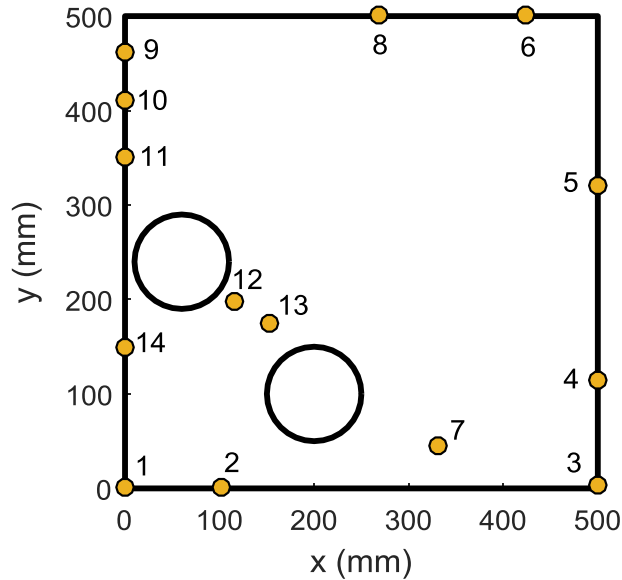


Figure 11. The selected sensor network on the square plate

Moreover, to verify the robustness of the results, a location sensitivity study is done on the square sandwich plate where we moved one sensor by a random distance and direction (between -0.5 cm and 0.5 cm in the x-direction and between -0.5 cm and 0.5 cm in the y-direction) and kept the other PZTs in their positions. This was repeated for 20 times and the coverage was calculated every time the sensor was moved. We then calculated the mean and standard deviation of the coverages obtained.

This procedure is done for all the sensors. Figure 12 shows the plot of the STD for each sensor. Indeed, all the standard deviations are very low. Thus, an error of 1 cm while installing sensors will have a minor effect on the coverage of the sensor network. This is expected in our cases where the coverage of the path is 30-40 mm on either side.

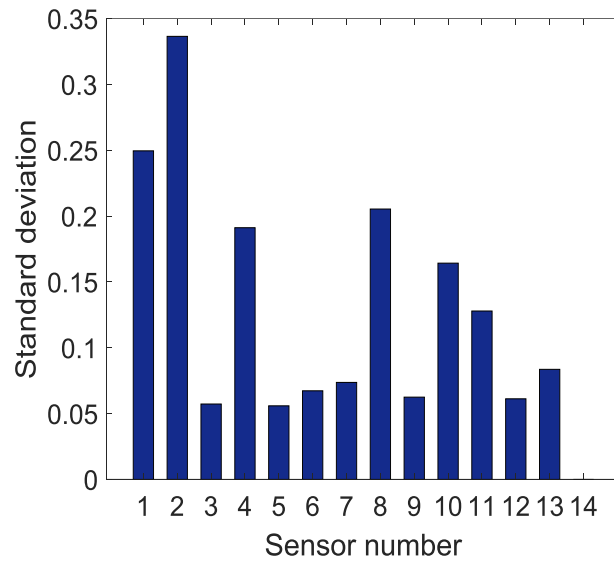


Figure 12. Standard deviation of the coverage when moving each sensor

B. Airbus A330 cargo door

The model was also validated on a large metallic structure, the cargo compartment door of an Airbus A330, shown in Figure 13. The cargo door is about 2740 mm by 2385mm and has a height of 501 mm and a total weight of 182.2 kg. Based on experimental analysis, it was demonstrated that the guided waves in this particular structure, excited at a relatively high frequency between 150 kHz and 300 kHz, have the ability to propagate with a minimum distance of 1-1.5 m and has a coverage of 30 mm, in this type of structures, based on an experimental investigation.

The optimization of the sensor network will be calculated on two bases (1) sub-structures and (2) the whole structure. Both methods will be elaborated on in the later sections.

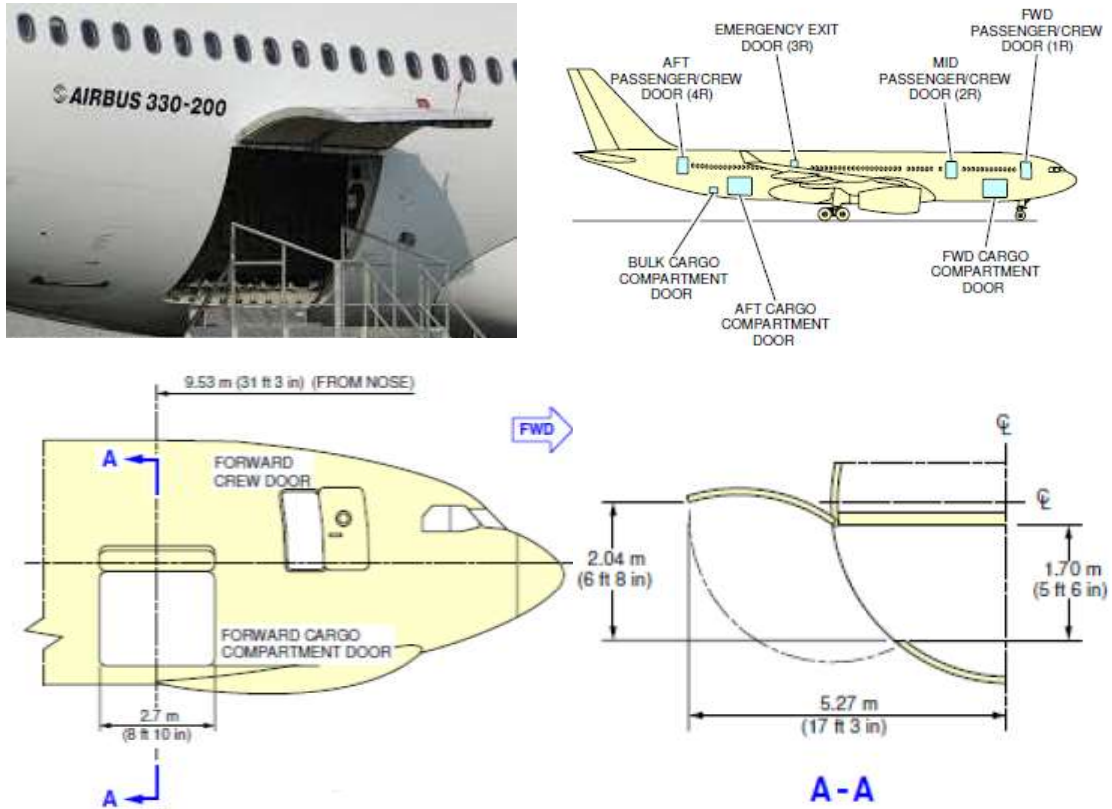


Figure 13. Airbus A330-200 cargo door position and dimensions [41]

1. Sub-structure optimization

The first method is based on subdividing the structure (the cargo door) into sub-structures. The optimization is then completed on each of the sub-structures before combining all the results in one network. For the structure under study, the cargo door was divided into 12 partitions (5 different geometries), as shown in Figure 14, where optimization was completed on each geometry alone.

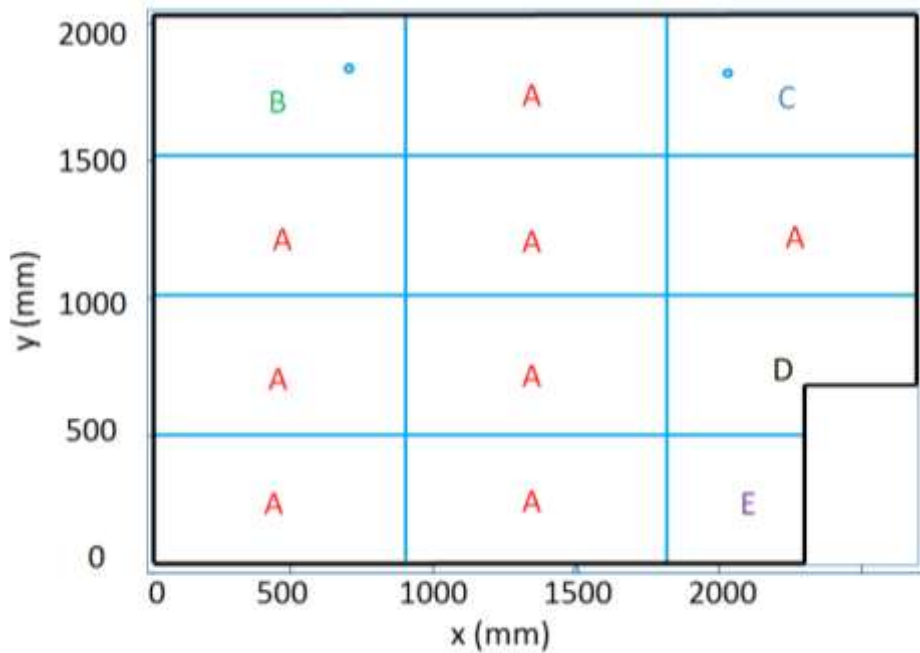


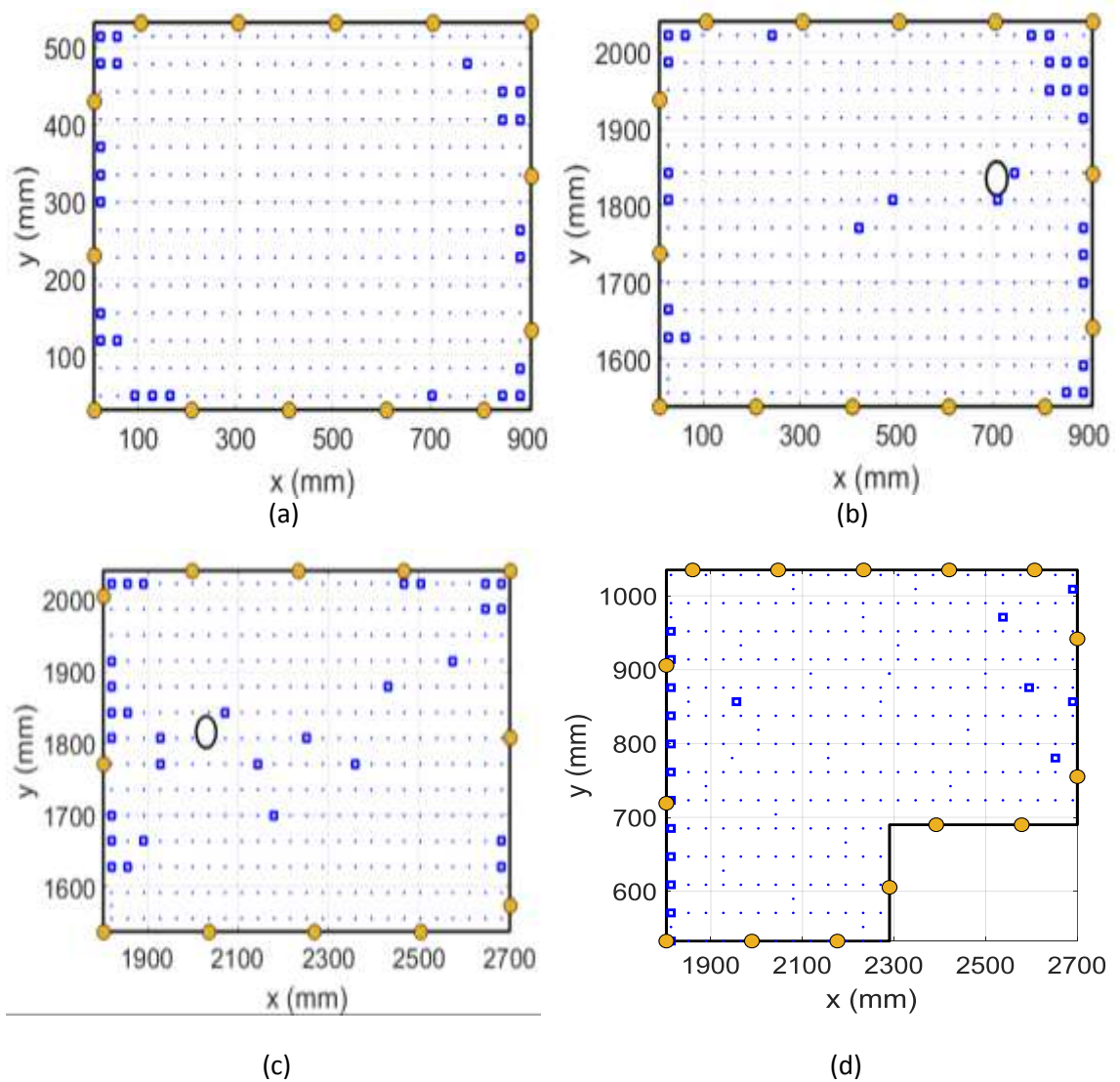
Figure 14. Cargo door partitions

The preliminary (PZT elements were uniformly distributed around the circumference) and optimized sensor networks of the partitions are shown in Figure 15 and Figure 16 respectively.

A total of 165 PZT wafers were needed, and they were able to provide a 99.825% coverage of the whole surface of the structure. The 165 PZTs were reduced further to 100 PZTs by replacing every 2 PZTs, separated by a distance less than 100 mm, by a PZT in between, resulting in a coverage of 99.3% (Figure 17 (a)). After that, a sensitivity study was completed to check the importance of each sensor. Each PZT wafer was assigned an importance value based on the coverage of the whole network in the case of its absence or failure, as described earlier. Each time, the least important sensor was removed, and the sensitivity study was repeated on the rest of the PZT

elements until only 70 sensors remained in the network resulting in a coverage of 90.5% (Figure 17 (b)).

The 70 sensors remaining in the network were taken as a preliminary solution for the whole structure, and then the optimization was performed. This has led to a significant improvement in the coverage reaching 94.5% (Figure 18 (a)).



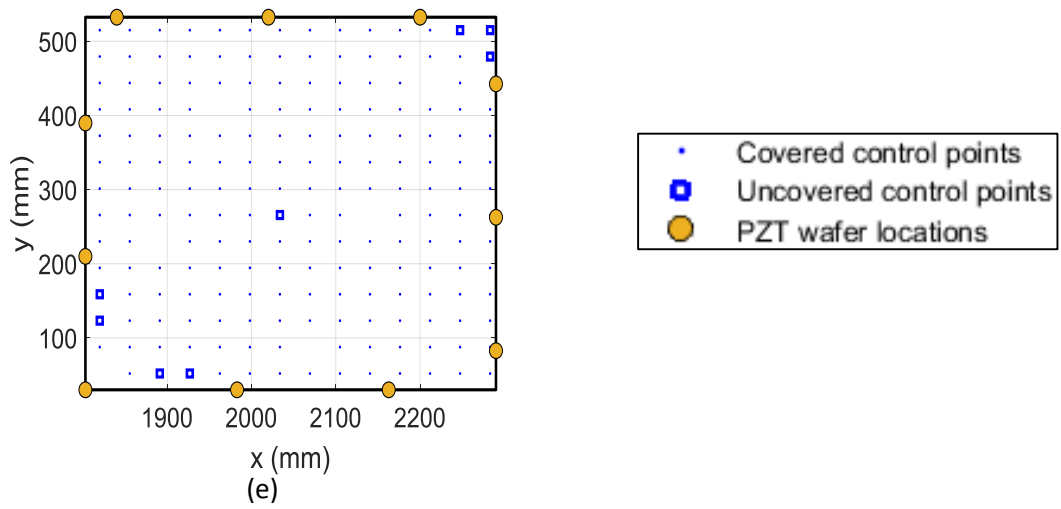
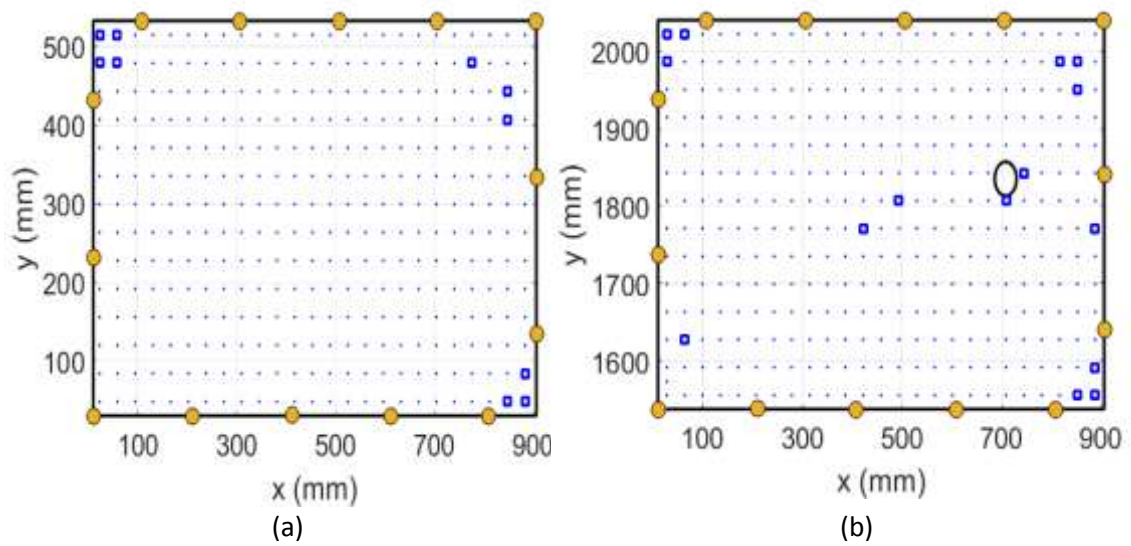
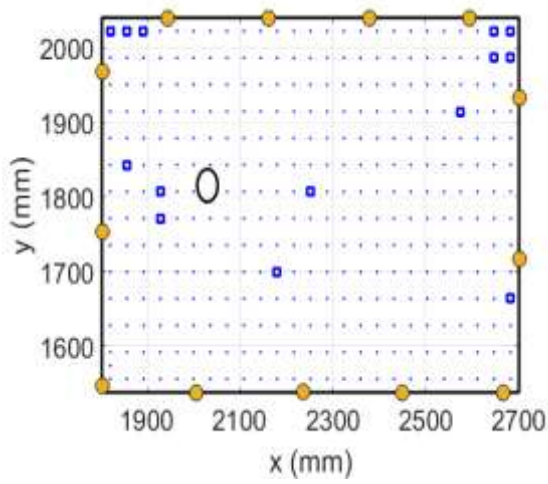
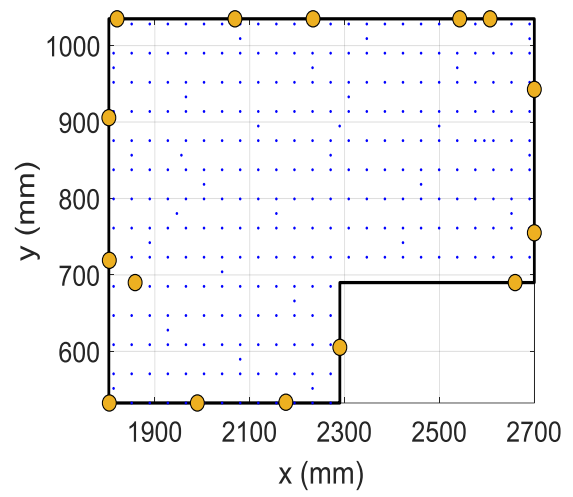


Figure 15. Preliminary sensor networks of: (a) partition A, (b) partition B, (c) partition C, (d) partition D, and (e) partition E

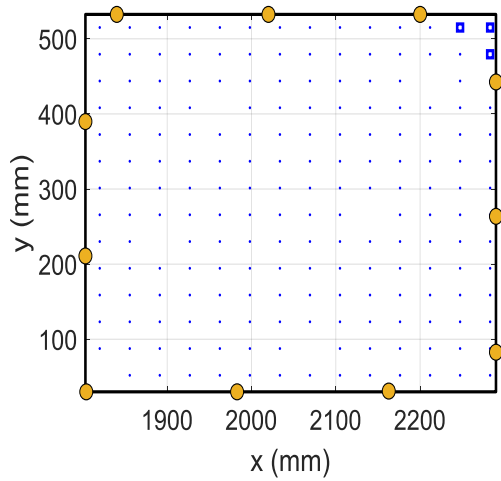




(c)



(d)



(e)

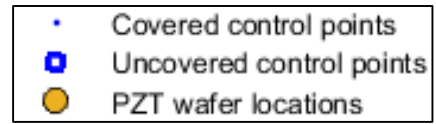
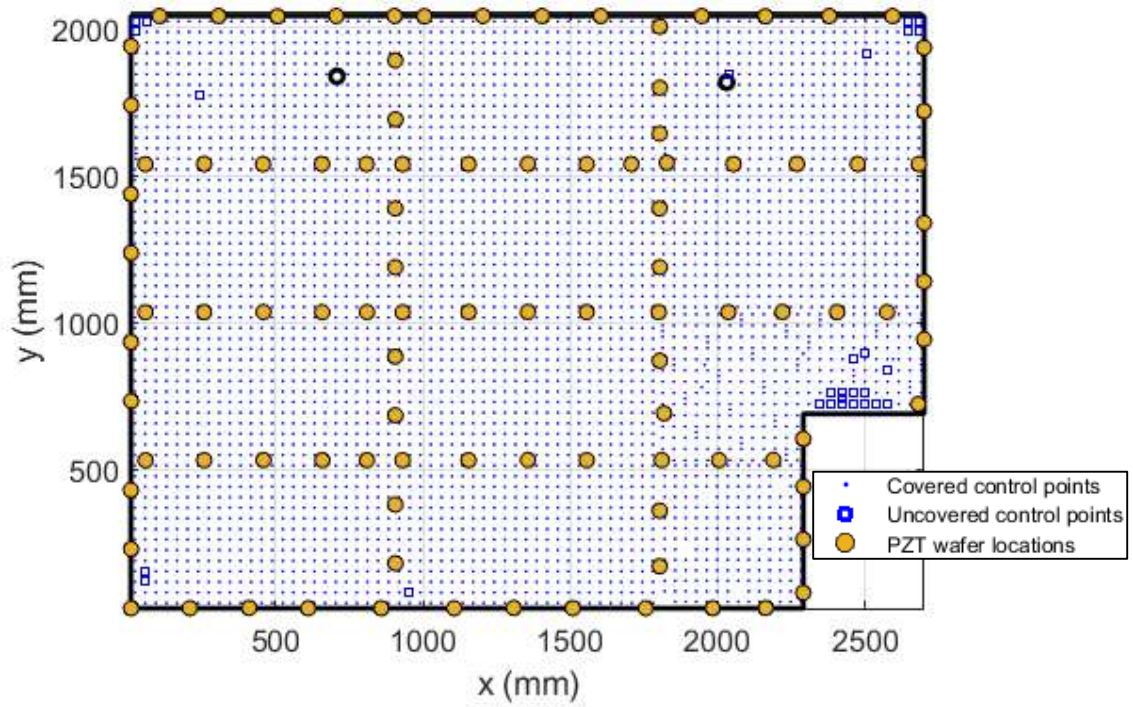
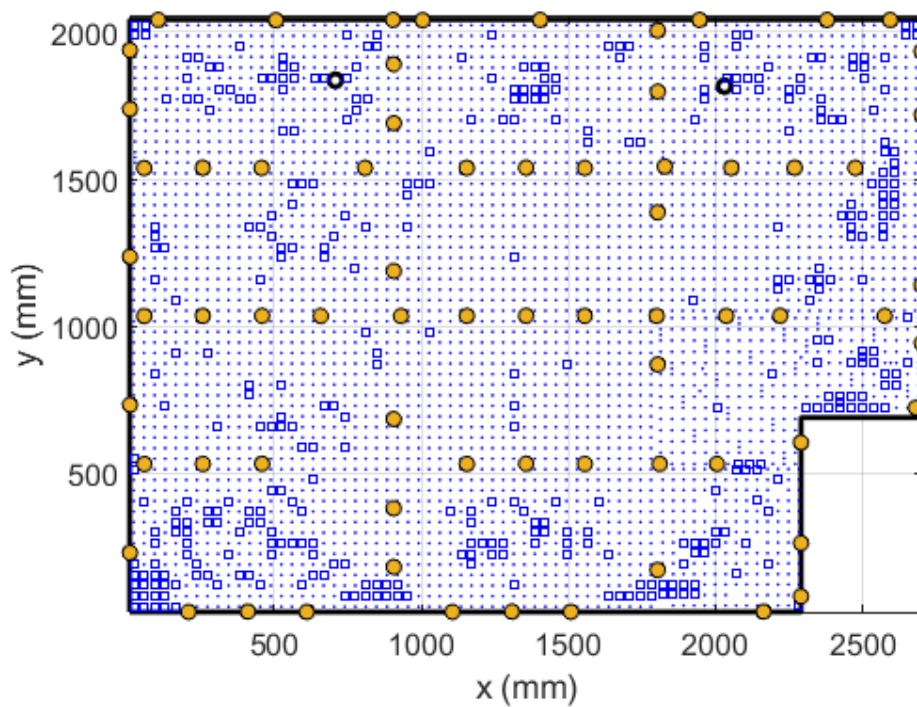


Figure 16. Optimized sensor networks of: (a) partition A, (b) partition B, (c) partition C, (d) partition D, and (e) partition E



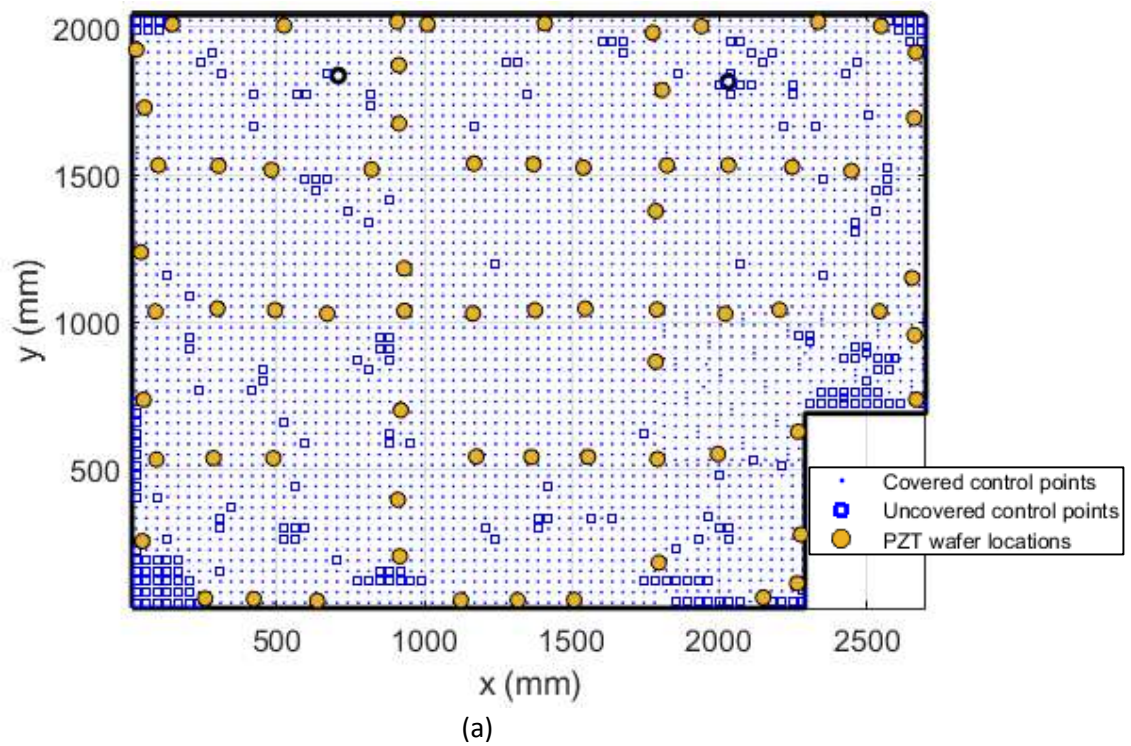
(a)



(b)

Figure 17. Combined sensor networks after reducing the PZTs from 165 to: (a) 100 sensors then (b) 70 sensors

The same work was repeated while keeping all parameters the same, however the propagation distance $d_{effective}$ was increased to 1.5 meters. The 94% coverage obtained using 70 PZTs, using a one-meter propagation distance, was achieved by 46 PZTs when increasing the propagation distance. This clearly shows the major effect of the propagation distance on the number of PZTs within the network. The two networks are displayed in Figure 18 (a) and Figure 18 (b).



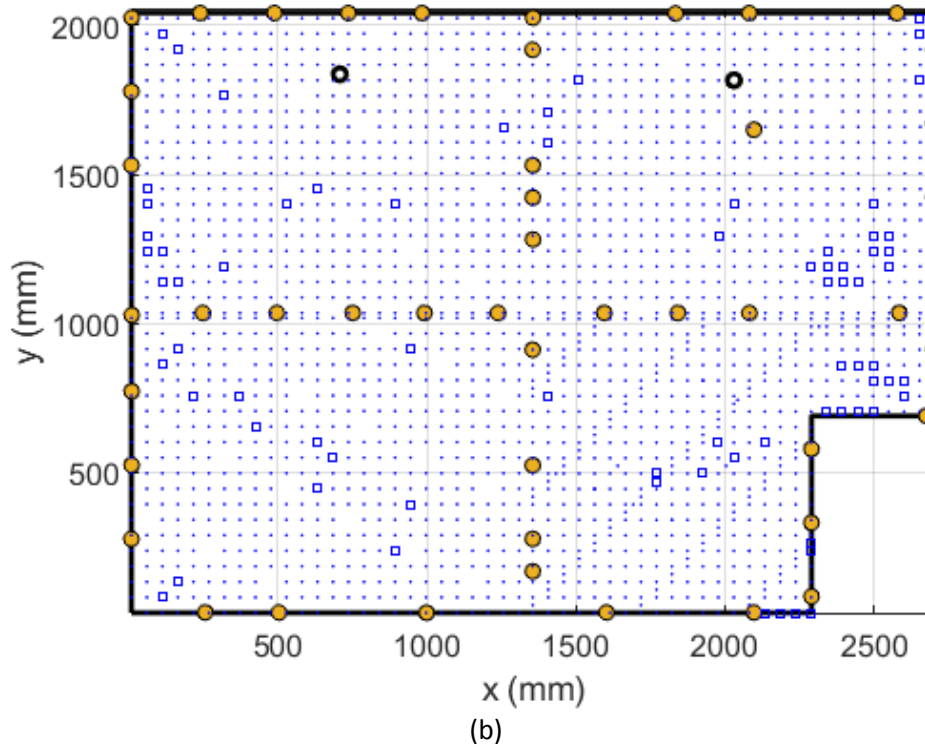


Figure 18. First approach's optimized sensor network, achieving 94% coverage, with a propagation distance and number of sensors of (a) 1 meter- 70 sensors and (b) 1.5 meters- 46 sensors

2. Optimization over the whole structure

This method completes the optimization over the entire surface rather than dividing it into partitions. Starting with the 70 sensors (based on the results of the previous method), the PZTs were uniformly distributed on the surface of the cargo door. The preliminary coverage was calculated to be 81%, as shown in Figure 19 (a). After performing the optimization (Figure 19 (b)), the results of the coverage improved by about 10% (optimized coverage = 90.35%). It can be concluded that the approach using the optimization over the substructure, may result in a slight improvement in the coverage. Feeding the optimizer by a good initial solution will ensure that the optimizer will not get stuck on a local optimum with poor coverage.

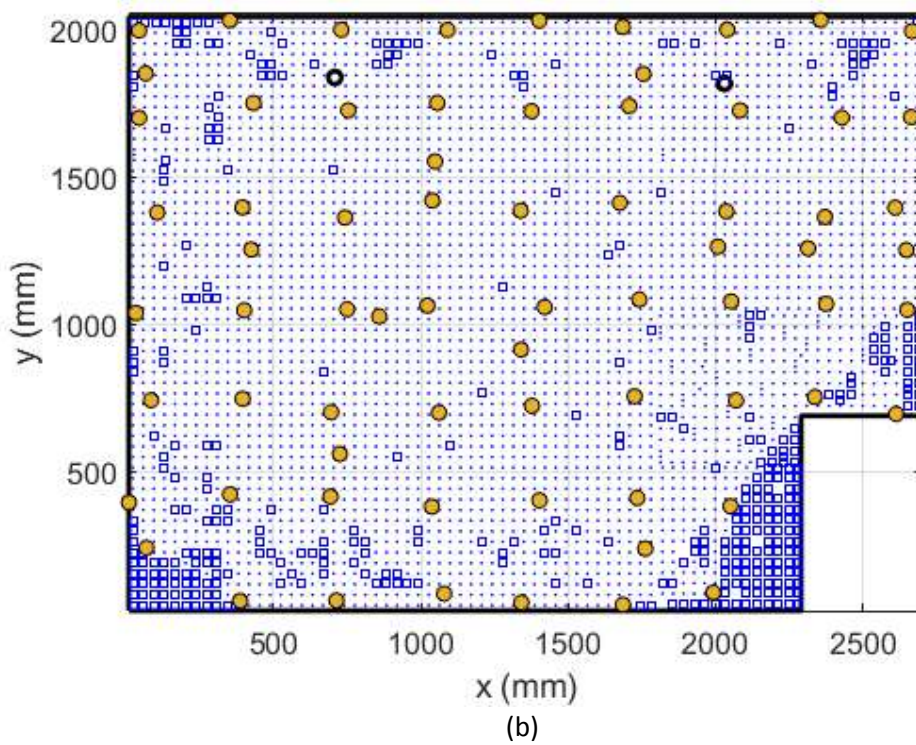
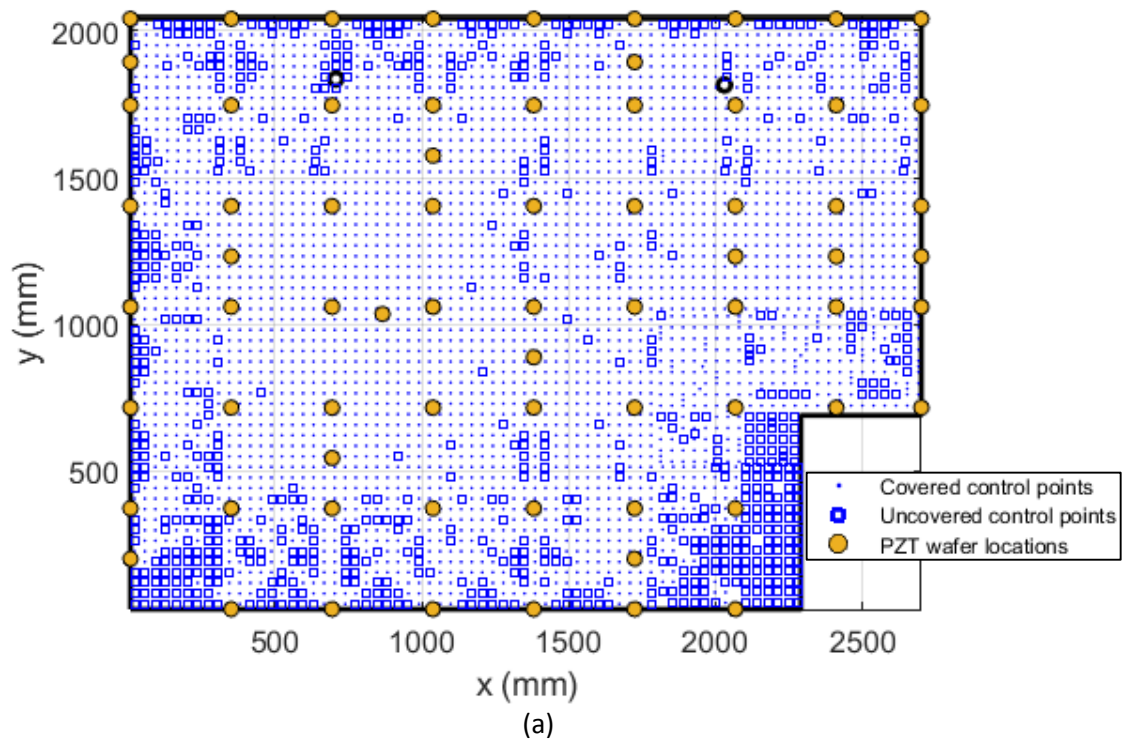


Figure 19. Second approach's 70-sensor networks: (a) preliminary and (b) optimized solutions

CHAPTER IV

EXPERIMENTAL VALIDATION

The experimental validation was carried on the composite sandwich square plate with the circular geometrical discontinuity, in addition to a section of the cargo door (section D). The main objective of the experimental work is to check the effectiveness of the optimized networks in damage localization. For this purpose, simulated damage was placed in several locations within the network, and the precision in damage localization was assessed.

A. Experiment set-up

1. Composite sandwich structure

A composite sandwich panel, measuring $600 \times 600 \text{ mm}^2$, was manufactured using a surface Carbon Fiber Epoxy (CF/EP) laminate which was made out of four woven plies in a quasi-isotropic configuration $[\pm 45, 0/90]_s$ with a nominal thickness of 0.88 mm, and high-performance foam core Dyvnicell HP100. The CF/EP laminate and the core were bonded together with FM 1515-3 film adhesive using secondary bonding in an autoclave. Two circular holes, 100 mm in diameter, were introduced into the plate to add the non-convex effect, as shown in Figure 20. The properties of the sandwich panels can be found in Mustapha et al. [40]. This sensor network was presented in Figure 5 (b).

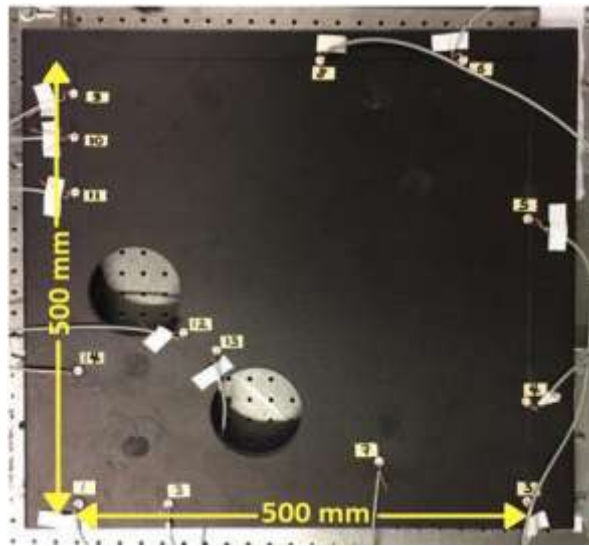


Figure 20. A photo of the tested composite sandwich plate

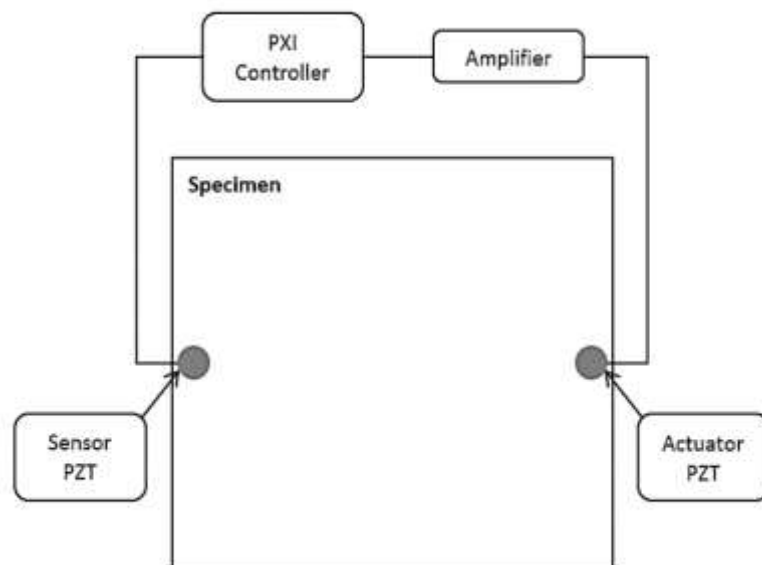


Figure 21. A schematic diagram of the experimental setup

The PZT wafers corresponding to the considered network configuration were mounted on the composite sandwich structure. Piezoelectric wafers, or PZTs, with wrapped electrodes (PI Ceramics, Lederhose, Germany), 10 mm in diameter and 1 mm in thickness were used. 5-cycle Hanning-windowed tone bursts were generated using an arbitrary wave generator (NI PXI-5422) at an excitation frequency of 200 and 250 kHz (at which the fundamental S_0 mode was dominant), sampled at a rate of 20 MSa/s. The generated signals were then amplified to 120 volts peak-to-peak voltage using an amplifier (EPA-104 Linear Amplifier, Piezo Systems Inc.), before being fed into the actuator PZT. While one PZT element functioned as the actuator to activate wave signals, the others functioned as sensors to capture the wave signals. The role of the actuator alternated until all the PZT elements had functioned as an actuator. The signals were captured using the NI PXIe-2593 multiplexer and the NI PXIe-5122 digitizer. All the modules were mounted on a PXIe-1082 chassis. Figure 21 shows a schematic diagram of the experimental setup.

Later, artificial damage was introduced by bonding a 200 grams steel block at three locations within the sensor networks. The same procedure explained above was repeated for each damage case, and the precision in damage localization was evaluated. Table 1 shows the coordinates of the 14 optimized locations of the PZT wafers.

Table 1. Optimized locations of the PZT wafers on the square panel

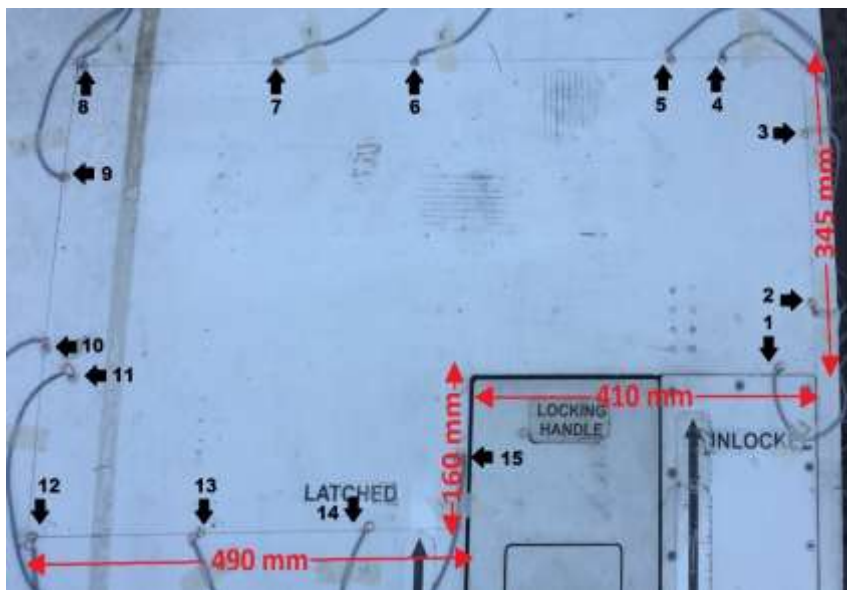
PZT number	X-coordinate	Y-coordinate
1	0	0
2	101	0
3	500	4
4	500	115
5	500	320
6	423	500
7	331	452
8	269	500
9	0	462
10	0	412
11	1	350
12	116	197
13	154	175
14	0	150

2. Airbus A330 cargo door

A section of the cargo (Partition D) was used to demonstrate the efficiency of the algorithm on metallic structures and is shown in Figure 22. The sensor network that will be used was presented in Figure 16 (d). Partition D will be tested because of its non-convex geometry. Fifteen PZT wafers were mounted on the structure, and artificial damage was introduced by bonding the 200 grams steel block at three locations within the sensor networks. The same experiment was done on the composite sandwich square plate (described earlier) was repeated on the cargo door but using an excitation frequency of 300 kHz. Table 2 shows the coordinates of the 15 optimized locations of the PZT wafers.



(a)



(b)

Figure 22. (a) Cargo door and (b) Section D sensor network

Table 2. Optimized locations of the PZT wafers on the cargo door

PZT number	X-coordinate	Y-coordinate
1	857	345
2	897	280
3	897	92
4	804	0
5	740	0
6	431	0
7	266	0
8	17	0
9	0	129
10	1	316
11	55	345
12	1	502
13	167	502
14	373	502
15	487	430

B. Experimental results

1. Data fusion

For each sensing path j , an anomaly value A_j (between 0 and 1) is assigned, reflecting the extent to which the path is affected by the damage. It is calculated via a direct comparison between the signals in the benchmark and damaged conditions based on the following:

$$A_j = 1 - \frac{\max(A_c)}{\max(A_i)} \quad (13)$$

where $\max(A_c)$ is the maximum amplitude of the current signal, and $\max(A_i)$ is the maximum amplitude of the healthy signal.

From the network of N PZT elements in the panel, $N \times (N - 1)$ sensing paths are available. Due to the dual function of the PZT elements, the number of paths can be reduced by half (e.g., instead of using both paths 1-6 and 6-1, only 1-6 can be considered). This value can be easily found by computing the number of possible combinations of 2 elements from a set of N distinct elements. After neglecting the collinear paths and those lying outside the geometry, the paths are further reduced to J relevant paths. The anomaly measures obtained for these J paths are employed to construct a damage image (using a data fusion technique). The damage location is expected to be located on the intersection of the most damaged paths, i.e., the paths having the highest anomaly measures.

After calculation of the anomaly measures of all J available paths, construction of the image damage is accomplished by dividing the monitored zone into a uniform grid of 1 mm^2 , where the existence of damage in each cell is evaluated by merging the perceptions of the anomaly measures from all the sensing paths. The DI or the probability of damage at a cell (x, y) in the observed zone is given by:

$$DI(x, y) = \sum_{j=1}^J P_j(x, y) = \sum_{j=1}^J A_j f_j(z) \quad (14)$$

where $P_j(x, y)$ is the probability of damage at cell (x, y) obtained from the anomaly measure of the j^{th} path; A_j is the anomaly measure for the j^{th} path; $f_j(z)$ is the normal distribution function for the j^{th} path (defined below).

To account for the possible existence of damage near the paths, the influence of the anomaly measure is considered in the shape of a normal distribution function

having a maximum effect on the path and decreasing away from it. This normal distribution function is defined by:

$$f(z) = \frac{1}{\sigma\sqrt{2\pi}} e^{-\frac{(z-\mu)^2}{2\sigma^2}} \text{ for } -\infty < z < +\infty \quad (15)$$

where μ is the mean of the normal distribution model and σ is its standard deviation.

Since the effect of a damage at a point located along the sensing path is stronger than a damage located at a certain distance from the sensing path, μ was set to be equal to zero.

On the other hand, the experimental investigation performed to determine the proper value of σ for the tested cargo door (aluminum structure), has found that the effect of a damage located at a point further than 30 mm from the sensing path is negligible. For this reason, σ was fixed at 30 mm. However, it was fixed at 40 mm for the sandwich structures based on literature [38]. Further, z was determined by assigning the same effect of damage for all the grid points that were equidistant from the path. This was conducted by considering a rectangular affected zone for each sensing path during the fusion process, where z was defined as the normal distance separating the grid point from the j^{th} sensing path.

To visualize the coverage of the used network for the grid, all the sensing paths were given similar weights instead of the anomaly values, and data fusion was applied for image reconstruction as explained earlier.

Due to the existence of strongly covered regions, with many sensing paths, the damage may be located within these regions because of the high damage indices of their

corresponding grid points. Therefore, the DI values at every grid element were normalized by the coverage of the same grid:

$$DI(x, y) = \frac{\sum_{j=1}^J P_j(x, y)}{\sum_{j=1}^J f_j(z)} = \frac{\sum_{j=1}^J A_j f_j(z)}{\sum_{j=1}^J f_j(z)} \quad (16)$$

2. *Damage localization- composite sandwich structure*

Damage images were constructed for the three damage locations. The actual and the predicted locations of the damage for the 200 kHz and 250 kHz are summarized in Figure 23 to Figure 25. It is clear that the precision, in damage localization, is high reaching a center distance of 10 mm between the actual and predicted damage. The accuracy in the prediction depends on the excitation frequency as well as the location of the damage within the sensor network. The maximum center distance obtained, between the actual and predicted damage, did not exceed 23 mm (case of damage 2, at 250 kHz), as indicated in Table 3.

It is evident that despite where the steel block was placed within the network, a reasonable prediction was achieved based on the data fusion and the optimized sensor network. Placing the simulated damage in a region that is uncovered as shown in Figure 26 (a), in the absence of PZTs 1, 12 and 13, was also investigated. The removal of the sensors resulted in an uncovered region in the left bottom corner. Damage is placed in the uncovered region (same position as damage 3) and the experimental validation was carried. After the data fusion, the simulated damage was not accurately predicted, as shown in Figure 26 (b). This further demonstrates the efficiency of GA in improving damage detection and localization.

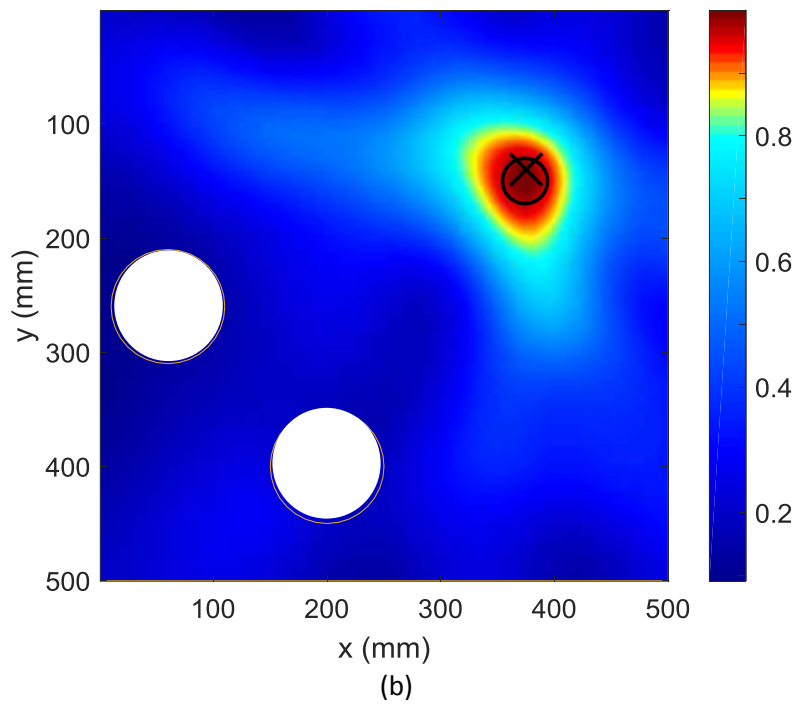
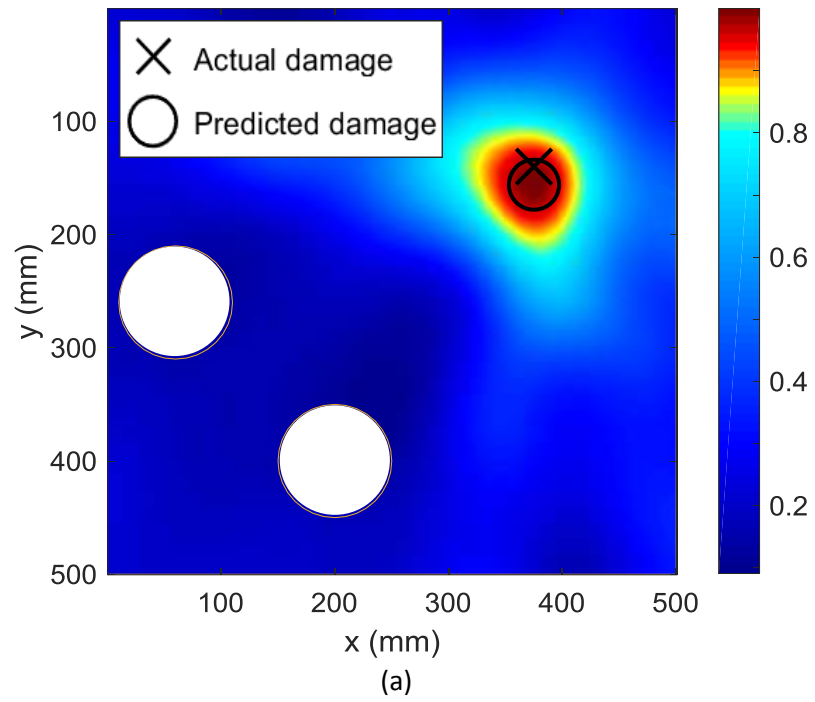


Figure 23. Damage localization of damage 1 on the square panel with the two circular holes at (a) 200 kHz and (b) 250 kHz

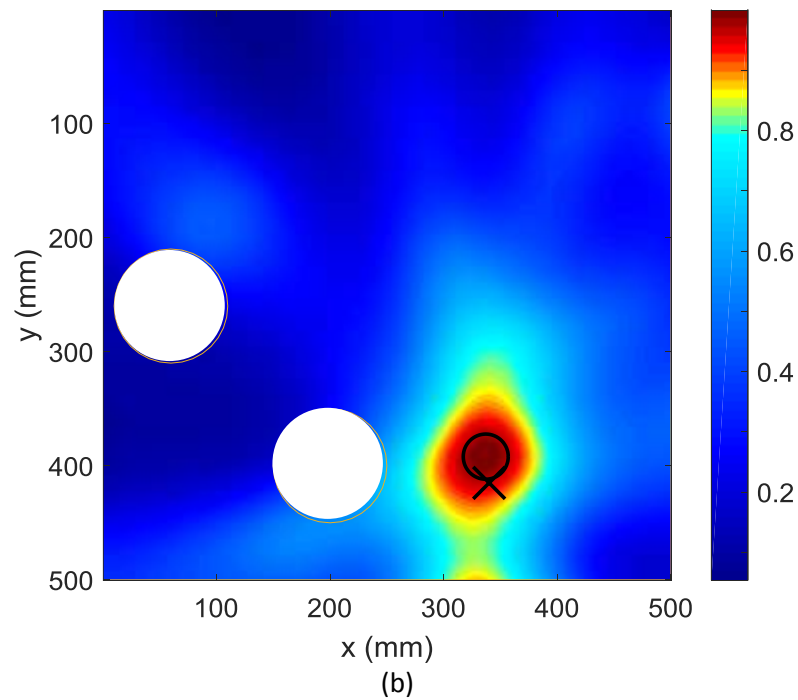
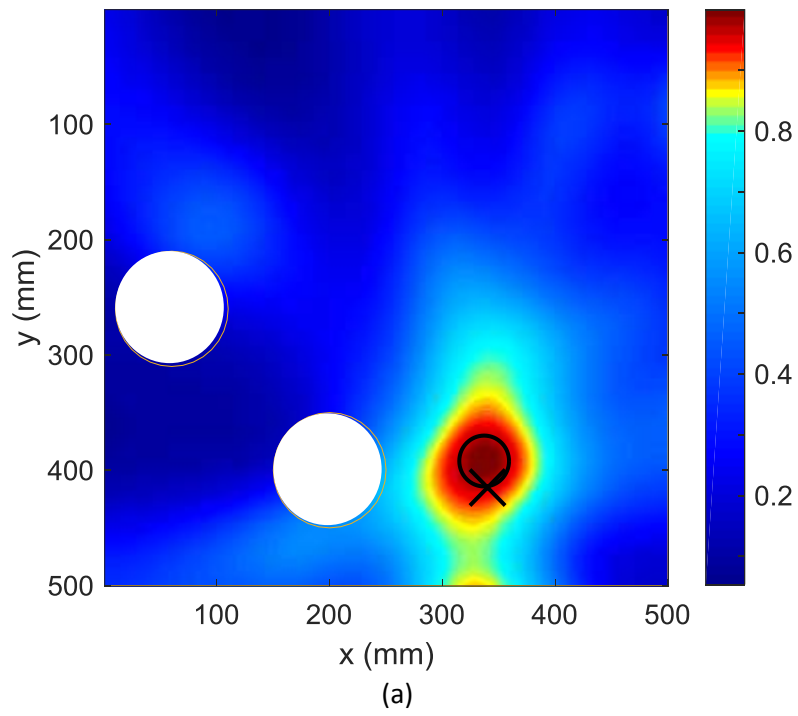


Figure 24. Damage localization of damage 2 on the square panel with the two circular holes at (a) 200 kHz and (b) 250 kHz

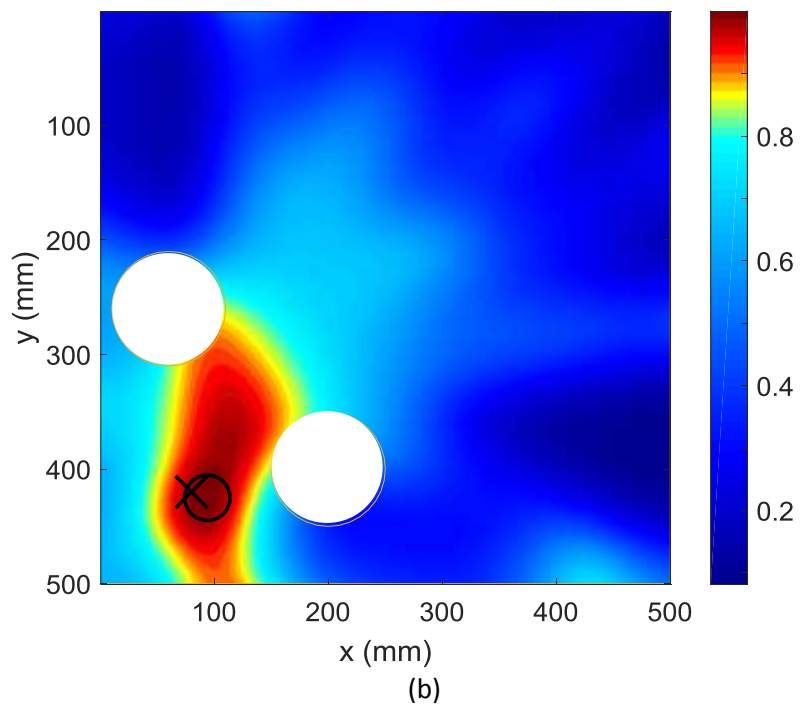
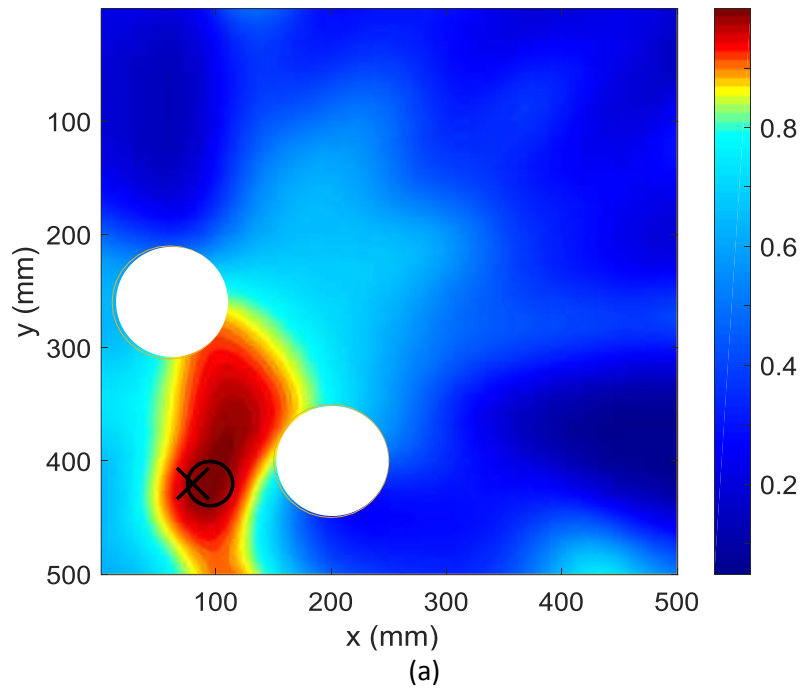
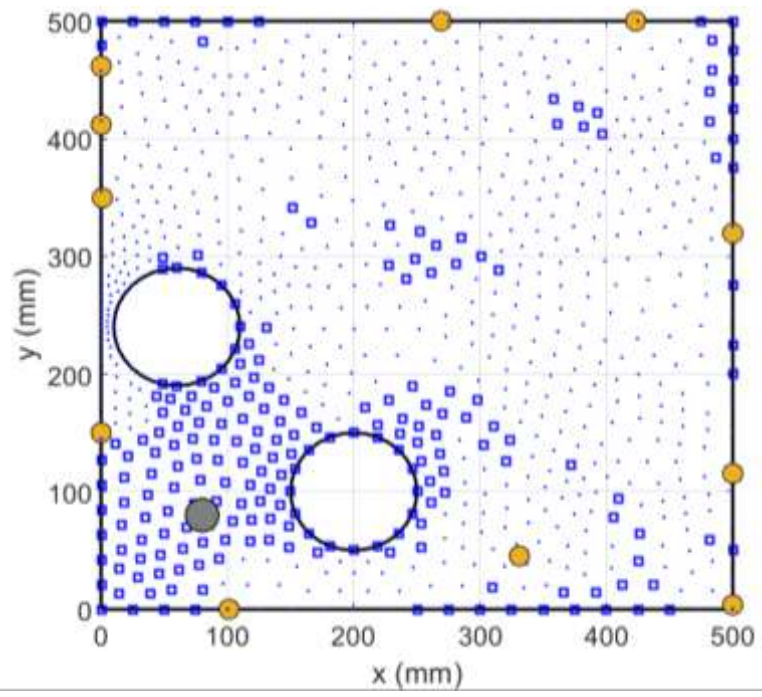
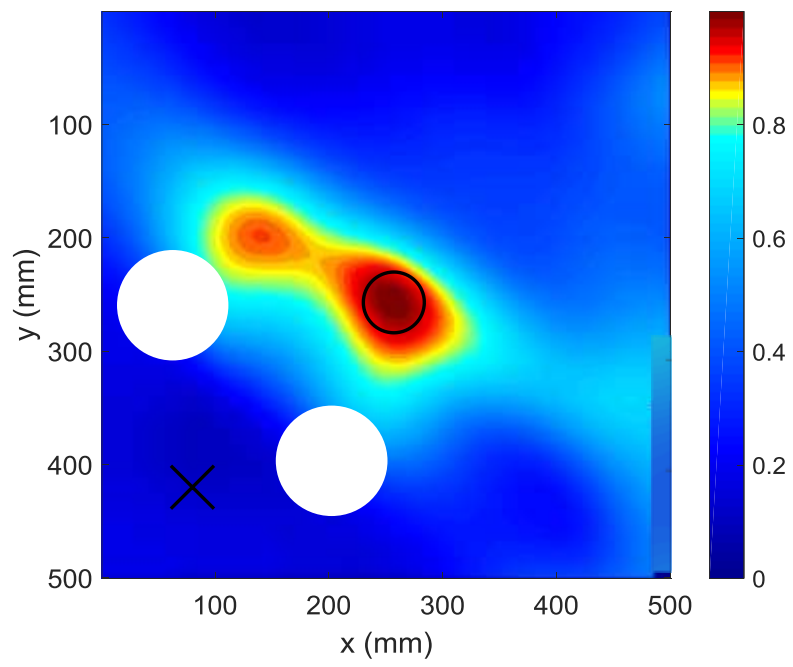


Figure 25. Damage localization of damage 3 on the square panel with the two circular holes at (a) 200 kHz and (b) 250 kHz



(a)



(b)

Figure 26. After removing some sensors: (a) the covered and covered regions, and (b) damage 3 prediction at 200 kHz

Table 3. Damage scenarios and predicted locations using an excitation frequency of 200 and 250

Sensor network	Square with 2 circular holes	
Excitation Frequency (kHz)	200	250
Actual Damage Location 1	(375,140)	(375,140)
Predicted Damage Location 1	(375,156)	(374,150)
Distance Variation (mm)	16	10
Actual Damage Location 2	(340,415)	(340,415)
Predicted Damage Location 2	(337,393)	(337,392)
Distance Variation (mm)	22	23
Actual Damage Location 3	(80,420)	(80,420)
Predicted Damage Location 3	(95,420)	(94,425)
Distance Variation (mm)	15	14.8

3. Damage localization- Airbus A330 cargo door

Similarly, the damage images were constructed for the tested cargo door partition. The actual and predicted locations of the damage, using an excitation frequency of 300 kHz, are summarized in Figure 27 to Figure 29. In a plate of maximum distance exceeding 1000 mm, the precision, in damage localization, is high giving a center distance values ranging from 11 to 40 mm between the actual and predicted damage (Table 4).

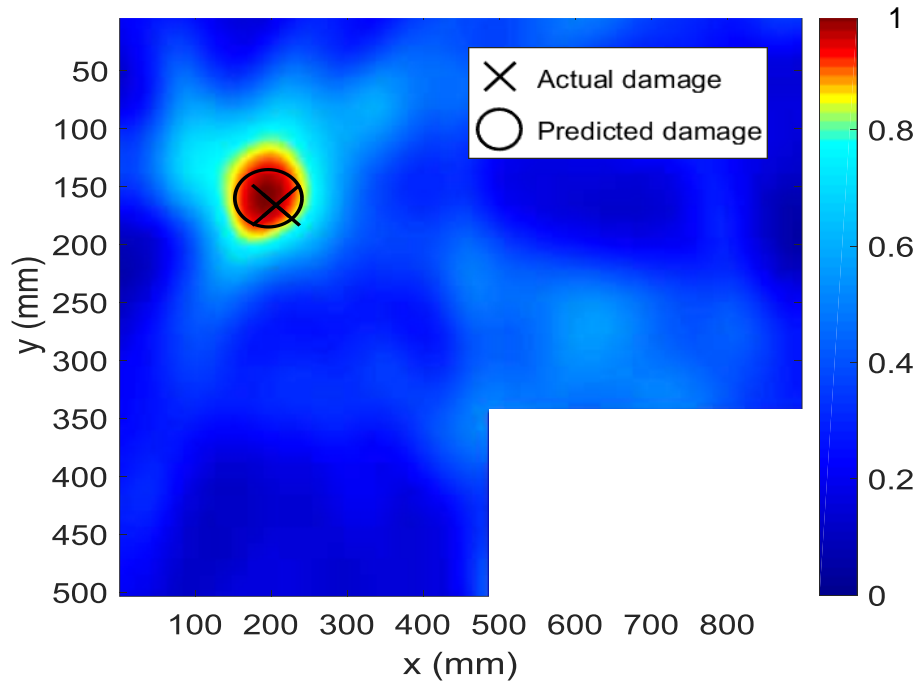


Figure 27. Damage localization, using an excitation frequency of 300 kHz on section D of damage 1

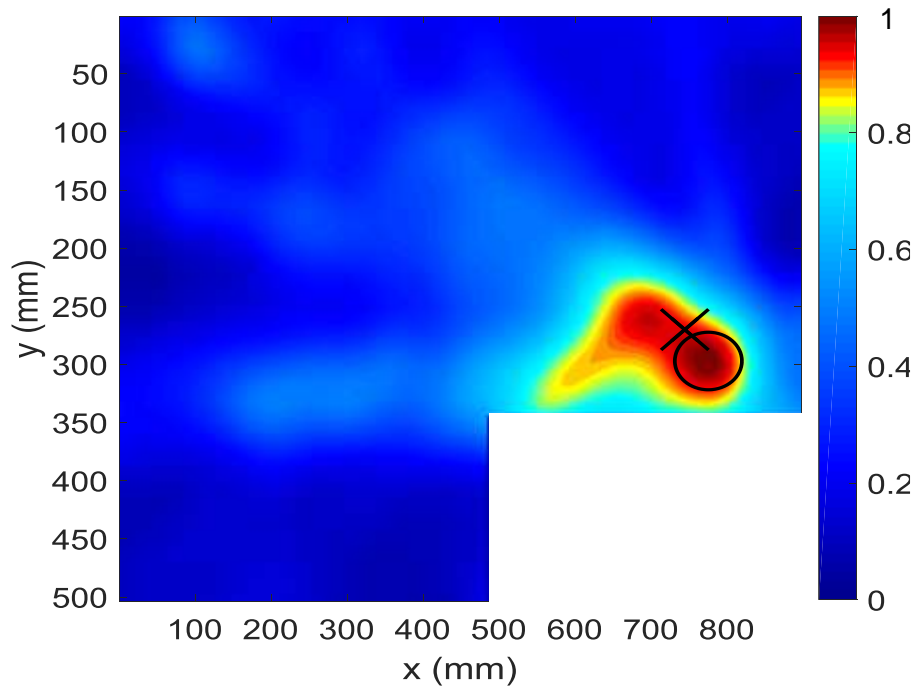


Figure 28. Damage localization, using an excitation frequency of 300 kHz on section D of damage 2

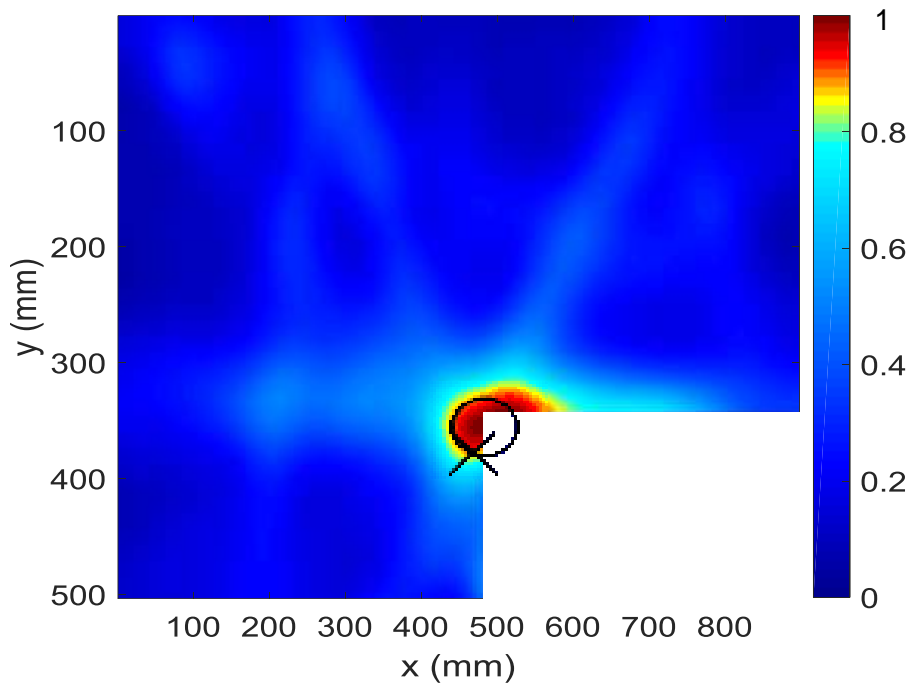


Figure 29. Damage localization, using an excitation frequency of 300 kHz on section D of damage 3

As proved, any surface can be tested in spite of its size, complexity, and non-convexity. For the same material properties, large and more complex geometries would require more sensors to provide adequate coverage. The addition of more sensors and control points is usually associated with an increase in computational time.

Table 4. Damage scenarios and predicted locations using an excitation frequency of 300 kHz

Sensor network	Cargo door
Excitation Frequency (kHz)	300
Actual Damage Location 1	(206,166)
Predicted Damage Location 1	(196,160)
Distance Variation (mm)	11.7
Actual Damage Location 2	(744,270)
Predicted Damage Location 2	(775,297)
Distance Variation (mm)	40
Actual Damage Location 3	(470,377)
Predicted Damage Location 3	(486,356)
Distance Variation (mm)	26

CHAPTER V

GRAPHICAL USER INTERFACE

A graphical user interface (GUI) was built for the developed model to facilitate its use and is made available for the user. Figure 37 shows a screenshot of the GUI which consists of 7 separated panels; 4 of them for the parameters and input, and 3 for optimization and results.

A. Geometry

The geometry panel is displayed in Figure 30. In this panel the user has the choice to enter the coordinates of the vertices of the polygon shape either directly or imported from an excel file. Using the drop down menu, the user can choose one of the two available options. In addition, the user specifies the number of control points in the assigned box. The more control points he puts; the more accuracy he gets. He should make a trade-off between accuracy and computational time. Then, the user can push the “Plot” button to generate the geometry, and the plot appears in the “Results and plots” panel. He can reset the geometry by clicking on “Reset geometry” button in case he wants to try another geometry.

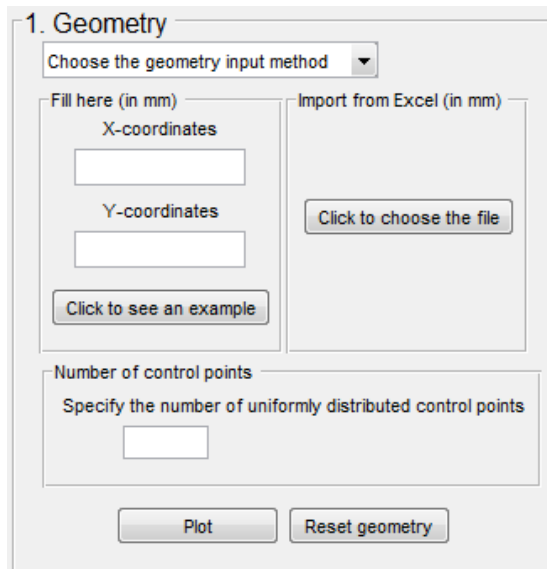


Figure 30. GUI- Geometry panel

B. Wave properties

In this panel (Figure 31), the user enters the wave properties in the material he is using. Those properties can be estimated for some popular materials or concluded from experiments. The panel is associated with a scheme that explains the mechanical meaning of each parameter.

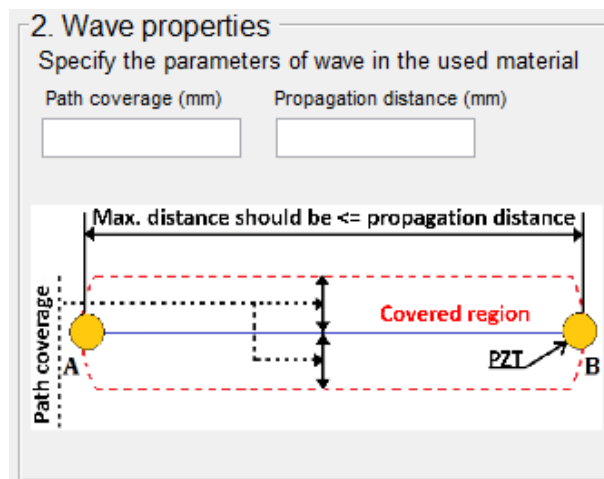
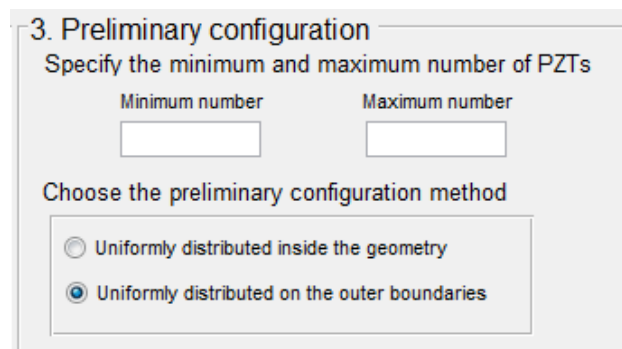


Figure 31. GUI- Wave properties panel

C. Preliminary configuration

The minimum and maximum number of PZT wafers should be specified by the user in this panel. Then, the preliminary configuration method can be chosen by clicking on one of two available radio buttons (Figure 32):

- Uniformly distributed inside the geometry
- Uniformly distributed on the outer boundaries.



3. Preliminary configuration

Specify the minimum and maximum number of PZTs

Minimum number	Maximum number
<input type="text"/>	<input type="text"/>

Choose the preliminary configuration method

Uniformly distributed inside the geometry

Uniformly distributed on the outer boundaries

Figure 32. GUI- Preliminary configuration panel

D. Aimed coverage

To specify the level of coverage (minimum number of paths to cover a point), the user should choose one of the options from the drop down menu. Then, the percentage of covered points required by the user should be specified in the empty box (See Figure 33).

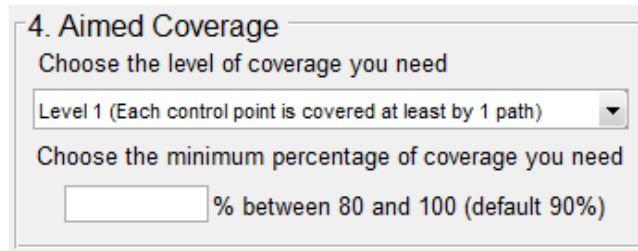


Figure 33. GUI- Aimed coverage panel

E. Optimization

The optimization panel consists of 3 push buttons as shown in Figure 34:

- “Optimize” to start the optimization
- “Pause” to stop the optimization
- “Resume” to continue the optimization

A wait bar is also included in this section to indicate that the application is working properly, and visualize the progression.

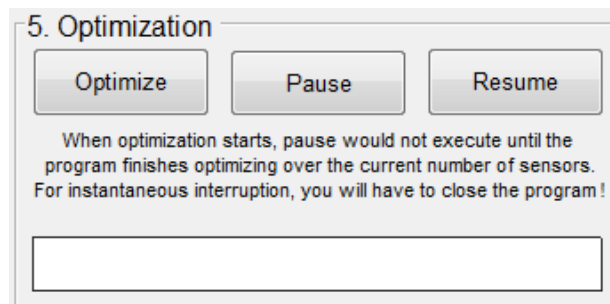


Figure 34. GUI- Optimization panel

F. Export results

This section has the following form (Figure 35):

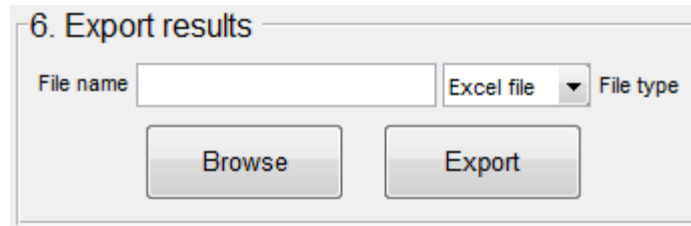


Figure 35. GUI- Export results panel

The user can export the optimized solution (PZTs coordinates) to an excel or text file by choosing from the drop down menu. The file name should be inserted in the empty box. The directory (file location) is chosen by clicking “Browse” push button; otherwise the file will be saved in the folder containing the application.

G. Results and plots

In this window (Figure 36), the minimum possible number of PZTs, the corresponding preliminary coverage, and the optimized coverage are displayed. In addition, 4 figures are plotted when clicking on “Plot solution” button: the geometry and control points figure, the preliminary configuration figure, the optimized solution figure, and another optimized solution figure with PZT importance indications where the PZTs colors range from the most important PZT (green) to the least important (red). The results and plots are erased when the user clicks on “Reset plots” button.

This section indicates if the solution is an optimal solution by glowing the “optimal solution” radio button. A solution is not optimal if the maximum number of PZTs can’t give the aimed coverage, or when the minimum number of PZTs is still giving coverage more than the required value.

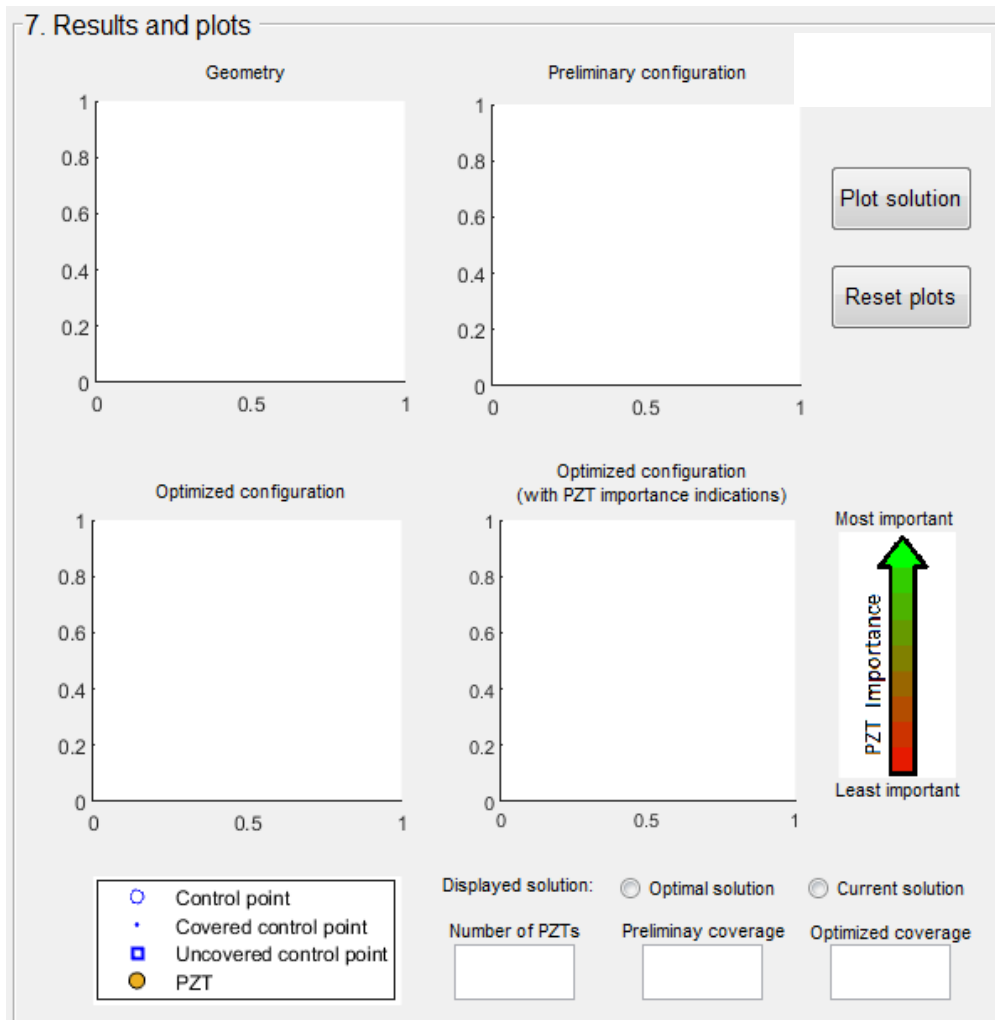


Figure 36. GUI- Results and plots panel

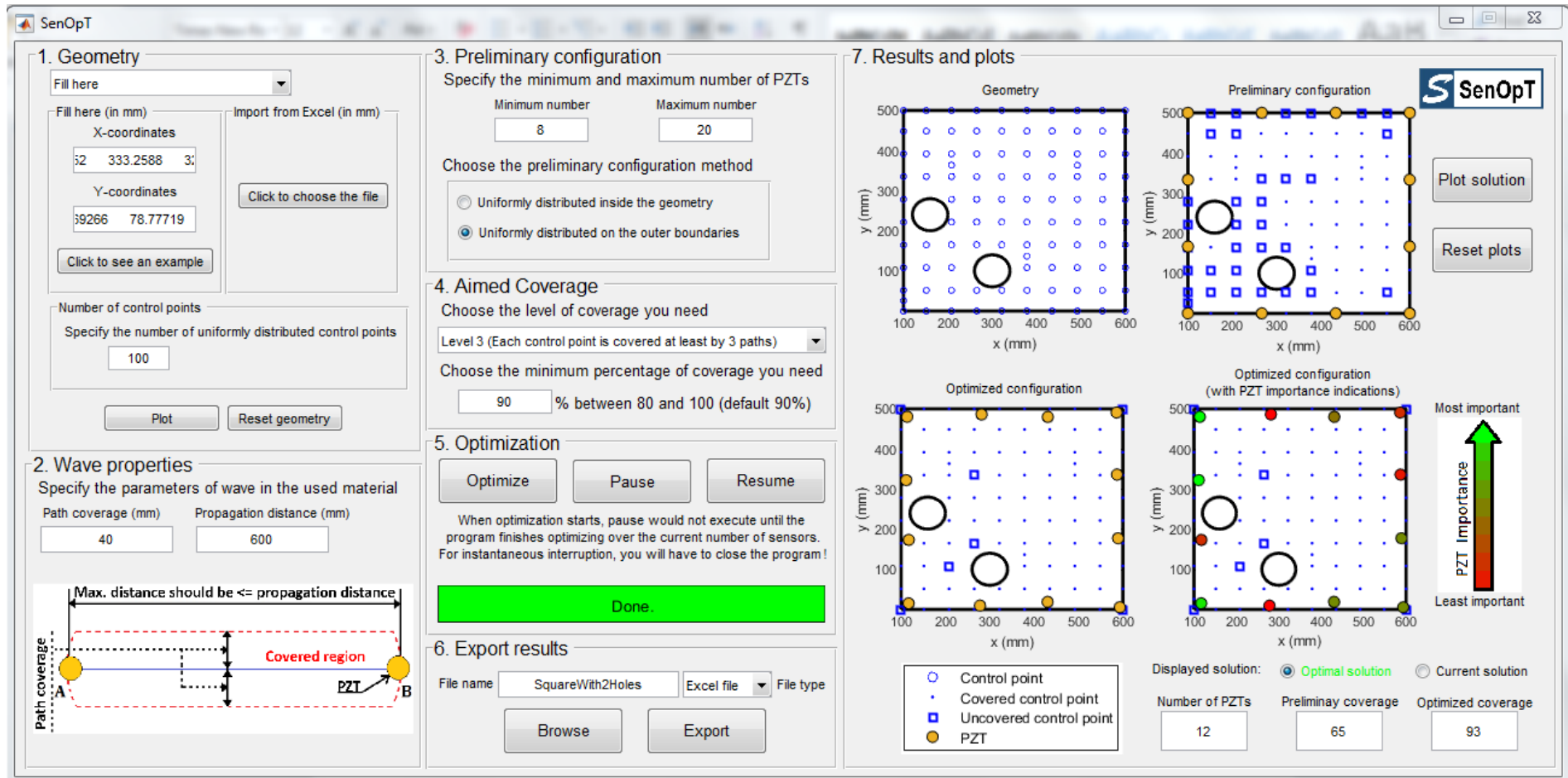


Figure 37. A screenshot of the GUI

CHAPTER VI

CONCLUSIONS

A novel approach for PZT-wafer-network placement, solved using GA, has been presented in this study. The proposed objective function was to maximize the coverage of the monitored area, represented by a set of control points while using the least possible number of sensors. Simulation results were presented for three cases, a square panel with geometrical discontinuity, a T-shaped panel, and a cargo door of an Airbus A330. The results showed a major improvement in the coverage level between the preliminary and optimized solutions. An optimized coverage of above 94% was achieved for the tested panels based on the minimized number of sensors while having the preliminary solution coverage less than 85% in all of the cases for the same minimized number of sensors. The repeatability of the results was demonstrated, and the variations in the solutions were minimal in most cases. In addition, experimental validation on the square panel and a part of the cargo door was performed using ultrasonic excitations at different frequencies. Artificial damages were detected and localized with an error not exceeding 4% of the maximal distance in the geometry.

Future work will include working on the interaction between sensor networks, i.e. transmitting data between distinct independent networks to cover large surfaces that a single network can't cover. Sensitivity study will be expanded, where real applications will be made to support high sensitivity sensors, by implementing several sensors in their

neighborhood. In addition, future work will include dealing with curved structures (tubular structures) and more complex three-dimensional structures taking into consideration the major difference in wave behavior between such structures and planar structures.

REFERENCES

1. Giurgiutiu, V., *Structural Health Monitoring with Piezoelectric Wafer Active Sensors: with Piezoelectric Wafer Active Sensors*. 2007, USA: Elsevier. 747.
2. Kessler, S.S., *Piezoelectric-based in-situ damage detection of composite materials for structural health monitoring systems*, in *Department of Aeronautics and Astronautics*. 2002, Massachusetts Institute of Technology. p. 140.
3. Ghajari, M., et al., *Identification of impact force for smart composite stiffened panels*. *Smart Materials and Structures*, 2013. **22**(8): p. 085014.
4. Chang, F.-K. and F. Kopsaftopoulos, *Structural Health Monitoring 2015: System Reliability for Verification and Implementation*. 2015, USA: DEStech Publications, Inc. 3166.
5. Gresil, M., A. Muller, and C. Soutis, *Acousto-ultrasonic Structural Health Monitoring of aerospace composite materials*. *Emerging Technologies in Non-Destructive Testing VI: Proceedings of the 6th International Conference on Emerging Technologies in Non-Destructive Testing (Brussels, Belgium, 27-29 May 2015)*. 2016: CRC Press. 109.
6. Raghavan, A., *Guided-wave structural health monitoring*, in *Aerospace Engineering*. 2007, University of Michigan.
7. Su, Z. and L. Ye, *Identification of damage using Lamb waves: from fundamentals to applications*. Vol. 48. 2009: Springer Science & Business Media. 345.
8. Dhillon, S.S. and K. Chakrabarty. *Sensor placement for effective coverage and surveillance in distributed sensor networks*. in *Wireless Communications and Networking, 2003. WCNC 2003. 2003 IEEE*. 2003. IEEE.
9. Padula, S.L. and R.K. Kincaid, *Optimization strategies for sensor and actuator placement*. 1999, NASA.
10. Bianchi, L., et al., *A survey on metaheuristics for stochastic combinatorial optimization*. *Natural Computing*, 2009. **8**(2): p. 239-287.
11. Battiti, R. and G. Tecchiolli, *Simulated annealing and tabu search in the long run: a comparison on qap tasks*. *Computers & mathematics with applications*, 1994. **28**(6): p. 1-8.
12. Chiang, W.-C. and C. Chiang, *Intelligent local search strategies for solving facility layout problems with the quadratic assignment problem formulation*. *European Journal of Operational Research*, 1998. **106**(2-3): p. 457-488.
13. Sinclair, M., *Comparison of the performance of modern heuristics for combinatorial optimization on real data*. *Computers & Operations Research*, 1993. **20**(7): p. 687-695.
14. Arostegui Jr, M.A., S.N. Kadipasaoglu, and B.M. Khumawala, *An empirical comparison of tabu search, simulated annealing, and genetic algorithms for facilities location problems*. *International Journal of Production Economics*, 2006. **103**(2): p. 742-754.

15. Paulli, J., *A computational comparison of simulated annealing and tabu search applied to the quadratic assignment problem*, in *Applied Simulated Annealing*. 1993, Springer. p. 85-102.
16. Hussin, M.S. and T. Stützle, *Tabu search vs. simulated annealing for solving large quadratic assignment instances*. IRIDIA, Université Libre de Bruxelles, 2010.
17. Jin, S., M. Zhou, and A.S. Wu. *Sensor network optimization using a genetic algorithm*. in *Proceedings of the 7th world multiconference on systemics, cybernetics and informatics*. 2003.
18. Heinzelman, W.R., A. Chandrakasan, and H. Balakrishnan. *Energy-efficient communication protocol for wireless microsensor networks*. in *System sciences, 2000. Proceedings of the 33rd annual Hawaii international conference on*. 2000. Maui, HI, USA, USA: IEEE.
19. Tillet, J., R. Rao, and F. Sahin. *Cluster-head identification in ad hoc sensor networks using particle swarm optimization*. in *Personal Wireless Communications, 2002 IEEE International Conference on*. 2002. India: IEEE.
20. Ostrovsky, R. and Y. Rabani, *Polynomial-time approximation schemes for geometric min-sum median clustering*. *Journal of the ACM (JACM)*, 2002. **49**(2): p. 139-156.
21. Bhondekar, A.P., et al. *Genetic algorithm based node placement methodology for wireless sensor networks*. in *Proceedings of the international multiconference of engineers and computer scientists*. 2009.
22. Lai, C.-C., C.-K. Ting, and R.-S. Ko. *An effective genetic algorithm to improve wireless sensor network lifetime for large-scale surveillance applications*. in *2007 IEEE Congress on Evolutionary Computation*. 2007. IEEE.
23. Yi, T.-H., H.-N. Li, and M. Gu, *Optimal sensor placement for health monitoring of high-rise structure based on genetic algorithm*. *Mathematical Problems in Engineering*, 2011. **2011**.
24. Guo, H., et al., *Optimal placement of sensors for structural health monitoring using improved genetic algorithms*. *Smart materials and structures*, 2004. **13**(3): p. 528.
25. Mallardo, V., Z. Sharif Khodaei, and F.M. Aliabadi, *A Bayesian approach for sensor optimisation in impact identification*. *Materials*, 2016. **9**(11): p. 946.
26. Flynn, E.B. and M.D. Todd, *Optimal placement of piezoelectric actuators and sensors for detecting damage in plate structures*. *Journal of Intelligent Material Systems and Structures*, 2010. **21**(3): p. 265-274.
27. Schoefs, F., E. Bastidas-Arteaga, and T.-V. Tran, *Optimal embedded sensor placement for spatial variability assessment of stationary random fields*. *Engineering Structures*, 2017. **152**: p. 35-44.
28. Worden, K. and A. Burrows, *Optimal sensor placement for fault detection*. *Engineering structures*, 2001. **23**(8): p. 885-901.
29. Mallardo, V., M. Aliabadi, and Z.S. Khodaei, *Optimal sensor positioning for impact localization in smart composite panels*. *Journal of intelligent material systems and structures*, 2013. **24**(5): p. 559-573.
30. Mallardo, V. and M. Aliabadi, *Optimal sensor placement for structural, damage and impact identification: A review*. *Struct. Durab. Health Monit*, 2013. **9**: p. 287-323.

31. Croxford, A.J., P.D. Wilcox, and B.W. Drinkwater. *Quantification of sensor geometry performance for guided wave SHM*. in *Health Monitoring of Structural and Biological Systems 2009*. 2009. San Diego, California, United States: International Society for Optics and Photonics.
32. Yi, T.H., H.N. Li, and C.W. Wang, *Multiaxial sensor placement optimization in structural health monitoring using distributed wolf algorithm*. *Structural Control and Health Monitoring*, 2016. **23**(4): p. 719-734.
33. Thiene, M., Z.S. Khodaei, and M. Aliabadi, *Optimal sensor placement for maximum area coverage (MAC) for damage localization in composite structures*. *Smart materials and structures*, 2016. **25**(9): p. 095037.
34. Cantero-Chinchilla, S., et al., *A robust Bayesian methodology for damage localization in plate-like structures using ultrasonic guided-waves*. *Mechanical Systems and Signal Processing*, 2019. **122**: p. 192-205.
35. Manohar, K., et al., *Data-Driven Sparse Sensor Placement for Reconstruction: Demonstrating the Benefits of Exploiting Known Patterns*. *IEEE Control Systems*, 2018. **38**(3): p. 63-86.
36. Zhang, H. and J.C. Hou, *On the upper bound of α -lifetime for large sensor networks*. *ACM Transactions on Sensor Networks (TOSN)*, 2005. **1**(2): p. 272-300.
37. Huang, C.-F. and Y.-C. Tseng, *The coverage problem in a wireless sensor network*. *Mobile networks and Applications*, 2005. **10**(4): p. 519-528.
38. Fakhri, M.A., et al., *Symbolic dynamics time series analysis for assessment of barely visible indentation damage in composite sandwich structures based on guided waves*. *Journal of Composite Materials*, 2017. **51**(29): p. 4129-4143.
39. Ismail, Z.M., et al., *The application of Genetic Algorithm for sensor placement of PZT wafers towards the application in structural health monitoring*, in *12th ENCNDT*. 2018, ECNDT: Gothenberg, Sweden.
40. Mustapha, S. and L. Ye, *Propagation behaviour of guided waves in tapered sandwich structures and debonding identification using time reversal*. *Wave Motion*, 2015. **57**: p. 154-170.
41. Airbus, S., *Airbus A380 aircraft characteristics airport and maintenance planning*. 2015, Issue Mar.

